Debottlenecking 4-hydroxybenzoate hydroxylation in *Pseudomonas putida* KT2440 improves muconate productivity from *p*-coumarate

Eugene Kuatsjah,[1,2] Christopher W. Johnson,[1] Davinia Salvachúa,[1] Allison Z. Werner,[1,2] Michael Zahn,[3] Caralyn J. Szostkiewicz,[1] Christine A. Singer,[1] Graham Dominick,[1] Ikenna Okekeogbu,[4] Stefan J. Haugen,[1] Sean P. Woodworth,[1] Kelsey J. Ramirez,[1] Richard J. Giannone,[2,4] Robert L. Hettich,[2,4] John E. McGeehan,[3] and Gregg T. Beckham[1,2*]

[1]Renewable Resources and Enabling Sciences Center, National Renewable Energy Laboratory, Golden, CO 80401, USA
[2]Center for Bioenergy Innovation, Oak Ridge National Laboratory, Oak Ridge TN 37830, USA
[3]Centre for Enzyme Innovation, School of Biological Sciences, Institute of Biological and Biomedical Sciences, University of Portsmouth, Portsmouth PO1 2DY, UK
[4]Biosciences Division, Oak Ridge National Laboratory, 1 Bethel Valley Rd, Oak Ridge, TN, 37830, USA

* *Corresponding Author Information:* gregg.beckham@nrel.gov

Abstract: The transformation of 4-hydroxybenzoate (4-HBA) to protocatechuate (PCA) is catalyzed by flavoprotein oxygenases known as *para*-hydroxybenzoate-3-hydroxylases (PHBHs). In *Pseudomonas putida* KT2440 (*P. putida*) strains engineered to convert lignin-related aromatic compounds to muconic acid (MA), PHBH activity is rate-limiting, as indicated by the accumulation of 4-HBA, which ultimately limits MA productivity. Here, we hypothesized that replacement of PobA, the native *P. putida* PHBH, with PraI, a PHBH from *Paenibacillus* sp. JJ-1b with a broader nicotinamide cofactor preference, could alleviate this bottleneck. Biochemical assays confirmed the strict preference of NADPH for PobA, while PraI can utilize either NADH or NADPH. Kinetic assays demonstrated that both PobA and PraI can utilize NADPH with comparable catalytic efficiency and that PraI also efficiently utilizes NADH at roughly half the catalytic efficiency. The X-ray crystal structure of PraI was solved and revealed absolute conservation of the active site architecture to other PHBH structures despite their differing cofactor preferences. To understand the effect *in vivo*, we compared three *P. putida* strains engineered to produce MA from *p*-coumarate (*p*CA), showing that expression of *praI* leads to lower 4-HBA accumulation and decreased $NADP^+$/NADPH ratios relative to strains harboring *pobA*, indicative of a relieved 4-HBA bottleneck due to increased NADPH availability. In bioreactor cultivations, a strain exclusively expressing *praI* achieved a titer of 40 g/L MA at 100% molar yield and a productivity of 0.5 g/L/h. Overall, this study demonstrates the benefit of sampling readily available natural enzyme diversity for debottlenecking metabolic flux in an engineered strain for microbial conversion of lignin-derived compounds to value-added products.

Keywords: muconic acid; aromatic catabolism; *Pseudomonas putida* KT2440; flavoprotein; metabolic engineering; *Paenibacillus* sp. JJ-1b; *para*-hydroxybenzoate hydroxylase; PraI; PobA

Abbreviations: PHBH, *para*-hydroxybenzoate-3-hydroxylase; 4-HBA, 4-hydroxybenzoate; PCA, protocatechuate; *p*CA, *p*-coumarate; FA, ferulate; MA, muconate

1. Introduction

Lignin valorization is critical for a competitive biomass-based economy (Becker and Wittmann, 2019; Corona et al., 2018; Davis et al., 2013; Huang et al., 2020). Lignin, however, presents challenges due to its inherent heterogeneity and complex structure (Beckham et al., 2016; Boerjan et al., 2003; Ragauskas et al., 2014). While biological lignin deconstruction and reassimilation are a part of the global carbon cycle, this process occurs over time scales that are incompatible with biomanufacturing (Becker and Wittmann, 2019). One potential approach to overcome this challenge is to combine chemo-catalytic lignin depolymerization and subsequent transformation of the lignin-derived aromatic intermediates to value-added products using microbial biocatalyst (Abdelaziz et al., 2016; Becker and Wittmann, 2019; Beckham et al., 2016; Liu et al., 2019a).

Pseudomonas putida KT2440 (hereafter *P. putida*) is a versatile bacterium capable of converting of heterogenous, lignin-derived aromatic compounds to a single product such as muconic acid (MA) or other target compounds (Almqvist et al., 2021; Johnson et al., 2019; Kohlstedt et al., 2018; Linger et al., 2014; Liu et al., 2019b; Notonier et al., 2021; Okamura-Abe et al., 2016; Presley et al., 2021; Ravi et al., 2017; Salvachúa et al., 2018; Salvachúa et al., 2015; Sonoki et al., 2018; Tumen-Velasquez et al., 2018; van Duuren et al., 2020; Vardon et al., 2015; Weimer et al., 2020). The genome of *P. putida* encodes multiple aromatic catabolic pathways, and strain development efforts benefit from robust genetic tools, making *P. putida* ideal for use in industrial processes (Ankenbauer et al., 2020; Belda et al., 2016; Jiménez et al., 2002; Martin-Pascual et al., 2021; Nikel et al., 2016a; Nikel and de Lorenzo, 2018; Nikel et al., 2014). Integrated bioprocess development and metabolic engineering approaches have enabled *P. putida* to transform lignin-related aromatic compounds such as *p*-coumarate (*p*CA) and ferulate (FA) to MA at a near theoretical yield (**Figure 1**) (Salvachúa et al., 2018). Subsequently, MA can be transformed into drop-in replacement dicarboxylic acids in polymers (Frost and Draths, 1995; Huo and Shanks, 2020; Lu et al., 2016; Shanks and Keeling, 2017; Vardon et al., 2015; Vardon et al., 2016), or used in performance-advantaged bioproducts (Carraher et al., 2017; Cywar et al., 2021; Vardon et al., 2016).

Techno-economic analysis has identified that MA productivity is a major hurdle for economic viability (Davis et al., 2018). This has been addressed to date by metabolic engineering, with examples including the introduction of genes associated with the production of prenylated flavin mononucleotide (prFMN) to boost the activity of the protocatechuate (PCA) decarboxylase, AroY (Johnson et al., 2016; Sonoki et al., 2014), the deletion of the Catabolite Repression Control protein gene, *crc* (Johnson et al., 2017), and over-expression of the native gene, *vanAB*, that encodes

O-demethylation of vanillate (Salvachúa et al., 2018). Additionally, adaptive laboratory evolution strategies were recently employed for an improved strain tolerance towards higher concentrations of *p*CA and FA (Mohamed et al., 2020). Despite these advances, the current strain performance remains below an industrially relevant level, which is in part due to the inefficiencies in several metabolic steps, including the conversion of 4-HBA (Salvachúa et al., 2018).

Para-hydroxybenzoate-3-hydroxylase (PHBH) catalyzes the hydroxylation of 4-HBA to PCA (**Figure 1**). Many previous studies have examined the PHBH mechanism, most notably with enzymes from *Pseudomonas aeruginosa* and *Pseudomonas fluorescens* (Entsch and Ballou, 1989; Entsch and Van Berkel, 1995; Howell et al., 1972; Husain and Massey, 1979). These studies have established PHBH as a paradigm for flavoprotein oxygenases (Ballou et al., 2005; van Berkel et al., 2006). PHBH employs a flavin adenine dinucleotide (FAD) cofactor to achieve catalysis by mediating the activation of molecular oxygen using reduced pyridine nucleotide (NAD(P)H) as a sacrificial electron donor to form the highly reactive flavin C4a-hydroxyperoxide species (Entsch and Ballou, 1989; Entsch et al., 2005; Hesp et al., 1969; Howell et al., 1972). Further, PHBH can be classified based on their preference towards nicotinamide cofactor (Westphal et al., 2018). The native PHBH from *P. putida*, PobA, belongs to the NADPH obligate cluster. By contrast, the other two clusters may utilize either NADPH or NADH and are distinguished by their relative preference between the two cofactors. One such PHBH that is promiscuous towards either forms of the pyridine nicotinamide cofactors, is PraI from *Paenibacillus* sp. JJ-1b, which has been used in systems such as an *Escherichia coli*-based biocatalyst for aromatic catabolism (Clarkson et al., 2017; Kasai et al., 2009).

In this work, we describe a strategy to relieve the metabolic bottleneck of 4-HBA transformation in a MA-producing strain of *P. putida* by replacing the endogenous PHBH, PobA, with PraI, which has a broader cofactor preference. We performed biochemical characterizations of PobA and PraI by comparing their kinetic parameters and determined the X-ray crystal structure of PraI in complex with 4-HBA and FAD. Engineered *P. putida* strains containing PobA only, PraI only, and a combination of both enzymes (**Figure 1**) were evaluated in shake flask experiments to compare their relative metabolite accumulation, intracellular PHBH concentrations, and nicotinamide cofactor ratios. Finally, the performance of the engineered strains was evaluated in bioreactor cultivations. Overall, this study provides insights that enable development of a more efficient biocatalyst to convert lignin-derived aromatics to MA from *p*CA.

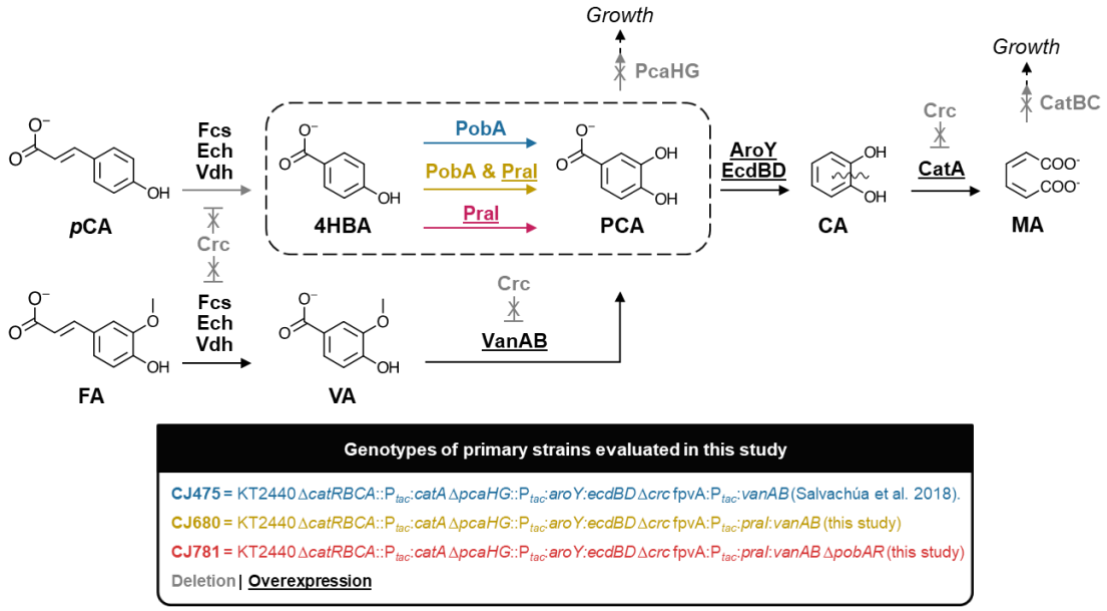

Figure 1. Metabolic pathway for the conversion of lignin-related aromatic compounds *p*CA and FA to MA in engineered *P. putida* strain CJ781. The key reaction considered in this work – 4-HBA hydroxylation to PCA – is highlighted in a dashed box. Engineered *P. putida* strains CJ475 (PobA only, blue), CJ680 (PobA and PraI, yellow), and CJ781 (PraI only, pink) harbor different combinations of PraI and PobA expression. Other engineered aspects, deletion, and overexpression of select genes are denoted in gray and underlined, respectively. Chemical abbreviations: FA, ferulate; *p*CA, *p*-coumarate; VA, vanillate; 4-HBA, 4-hydroxybenzoate; PCA, protocatechuate; CA, catechol; MA, muconate.

2. Material & Methods

2.1. Plasmid construction

We used Q5® Hot Start High-Fidelity 2X Master Mix or Phusion (New England Biolabs) for all polymerase chain reactions (PCR). NEBuilder® HiFi DNA Assembly Master Mix or Gibson assembly master mix (New England Biolabs) were used to assemble plasmids, followed by transformation into NEB® 5-alpha F'I^q competent *E. coli* cells (New England Biolabs). All plasmids were confirmed by Sanger sequencing (GENEWIZ). **Table S2** contains detailed

plasmid construction information, **Table S3** contains the sequence of the synthesized DNA fragment containing the *praI* gene, and **Table S4** contains the sequence of the oligos used in plasmid and strain construction.

2.2. Protein expression and production

The plasmids pEUK018, pEUK019, and pEE003 which encode for *tagless* PobA (PP_3537), PraI (BAH79107), and C'-polyHis-tagged PraI (BAH79107), respectively, were used to transform λ(DE3) *E. coli* for heterologous protein production. PobA was produced using BL-21 λ(DE3) and lysogeny broth (LB Miller, 10 g/L tryptone, 5 g/L yeast extract, 10 g/L NaCl) containing ampicillin (100 mg/L). Both versions of PraI were produced using terrific broth (TB, 20 g/L tryptone, 24 g/L yeast extract, 4 mL/L glycerol, 17 mM KH_2PO_4, and 72 mM K_2HPO_4) supplemented with ampicillin (100 mg/L) and chloramphenicol (30 mg/L). The starter cultures were grown from a single colony of *E. coli* transformed with appropriate plasmids (or an equivalent glycerol stock, *vide supra*) were grown overnight in LB (Miller) with the appropriate antibiotics. 10 mL of the starter culture was used to inoculate a 2.5 L baffled flask containing 1 L of LB (PobA) or TB (PraI) with antibiotics and grown at 37°C, 225 rpm. The cultures were induced at an OD_{600} of ~0.7 with 1 mM IPTG and 0.2 mM of riboflavin; additionally, 1 mg/mL of biotin was added to cultures producing PraI. Subsequently, the cultures were grown for an additional 16 – 18 hours at 20°C, 225 rpm. The resulting biomass was collected by centrifugation and frozen at -80°C until further use.

Tagless PobA and PraI were used for kinetic analyses and the PraI-His was used for protein crystallography. For purification, thawed biomass was suspended in an equivalent volume of 20 mM HEPES, 100 mM NaCl, pH 7.5 containing a trace amount (~1 mg) of DNAseI and lysed by sonication. The cell lysate was cleared by centrifugation and passage through a 0.45 µm filter. *Tagless* PobA and PraI were purified using a combination of $(NH_4)_2SO_4$ precipitation, hydrophobic interaction chromatography, and anion exchange chromatography. The chromatographic purification of PobA and PraI was assisted by the yellow-coloration of their flavin cofactor and was performed using an ÄKTA Pure Fast protein liquid chromatography (FPLC) system (Cytiva) using 20 mM HEPES, 100 mM NaCl, pH 7.5 as the buffer A. 1 M $(NH_4)_2SO_4$ was added to the cleared lysates, and the precipitated proteins were removed by centrifugation. The soluble protein fraction was injected into a column containing Source-15 Phenyl resin (Cytiva) with a gradient of 1 – 0 M $(NH_4)_2SO_4$ in 120 mL. Fractions containing PobA or PraI were pooled, dialyzed into buffer A, and injected into a column containing Source-15 Q resin (Cytiva) with a gradient of 0.1 – 0.5 M NaCl in 60 mL. The PraI-His was purified using HisTrap column (Cytiva) and washed with up to 20 mM imidazole. The PraI-His eluate was subjected to anion exchange chromatography in the similar manner as its *tagless* counterpart. Fractions containing PobA or PraI were pooled, dialyzed into buffer A, frozen as beads in liquid N_2, and stored at -80°C. For crystallization, PraI-His was further purified with size-exclusion chromatography and eluted as a dimer into 20 mM Tris pH 8.0 and 150 mM NaCl.

2.3. Steady-state kinetic analysis

The hydroxylation of 4-HBA was monitored continuously by following the consumption of the co-substrates NAD(P)H or O_2. NAD(P)H consumption was monitored using a Cary 4000 UV-Vis spectrophotometer (Agilent) connected to a Peltier device at 340 nM (ε_{340} = 6 mM^{-1} cm^{-1}); O_2 consumption was monitored using a Clark-type electrode oxygraph OXYG1+ (Hansatech) connected to a circulating water bath and calibrated using air-saturated water and $Na_2S_2O_4$ according to the manufacturer's instructions. The standard assay was performed in air-saturated 50 mM Tris/SO_4 pH 8 supplemented with 60 µM FAD at 25°C and initiated by the addition of 20 nM of PobA or PraI. Initial velocities were measured as a function of the NAD(P)H, 4-HBA, or O_2 concentrations. 300 µM of NAD(P)H and 200 µM of 4-HBA were used when varying the O_2 concentration, and when varying the 4-HBA or NAD(P)H concentrations. NAD(P)H consumption assays were used when varying the concentrations of 4-HBA or NAD(P)H; and O_2 consumption assays were used when individually varying the concentrations of all three substrates. Different starting O_2 concentrations were achieved by bubbling N_2 gas into the buffer prior to sealing the oxygraph chamber and initiating the reaction. The initial O_2 concentrations were normalized to the ambient air-saturated buffer in between runs. The steady-state kinetic parameters were obtained by fitting the Michaelis-Menten equation to the data using Leonora (Cornish-Bowden, 1995).

2.4. Reaction stoichiometry

Molar balances of the reactants and products in the PHBH-catalyzed reactions were evaluated using the combination of oxygraph, spectrophotometer, and HPLC-based assays. An end-point assay was performed in air-saturated 50 mM Tris/SO_4 pH 8 without FAD supplementation at 25ºC. The mixture also contained 100 µM 4-HBA, 300 µM NAD(P)H, and the reaction was initiated by the addition of 2 µM PobA or PraI. The reaction was run to completion by the depletion of 4-HBA and the total O_2 consumed during this process was monitored in an oxygraph. Finally, the concentration of PCA produced was monitored on a high-performance liquid chromatography (HPLC) compared to authentic standards as described in *section 2.11*. The data were reported as an average of three independent replicates.

2.5. Protein crystallography

PraI-His was concentrated to 10 mg/mL and sitting drop co-crystallization trials with 1 mM 4-HBA were set up with a Mosquito crystallization robot (SPT Labtech) using SWISSCI 3-lens low profile crystallization plates. Crystals grew in condition A3 (20% PEG3350 and 0.2 M ammonium citrate dibasic) of the JCSG Plus screen (Molecular Dimensions) and were further optimized by hanging drop vapor diffusion using EasyXtal 15-well tools plates (Qiagen). Crystals were cryo-cooled in liquid nitrogen following the addition of 20% glycerol to the crystallization solution. Diffraction data were collected on beamline I03 at the Diamond Light Source (Didcot, UK) and automatically processed with STARANISO (Tickle et al., 2018) on ISPyB. The structure was solved within CCP4 Cloud by molecular replacement with Phaser (McCoy et al., 2007) using a search model created by the Phyre2 server (Kelley et al., 2015). Model building was performed in Coot (Emsley et al., 2010)

and the structure was refined with BUSTER (Bricogne et al., 2017). MolProbity (Williams et al., 2018) was used to evaluate the final model and PyMOL (Schrödinger, LLC) for protein model visualization. Data and Refinement statistics are summarized in **Table S5**. The atomic coordinates have been deposited in the Protein Data Bank and are available under the accession code 7ON9. The Dali server (Holm, 2020) was used to find the closest structural homologs for PraI. The determination of secondary structure elements is performed using DSSP (Kabsch and Sander, 1983; Touw et al., 2015).

2.6. Strain construction

Competent *P. putida* cells for electroporation were prepared following the procedure described previously (Choi et al., 2006). Plasmid DNA (300-500 ng) was transformed into competent *P. putida* cells (50 μL) using electroporation methods (Choi et al., 2006). Cells were recovered in 950 μL SOC for 1-2 hours at 30°C, 225 rpm. Following the recovery period, the culture was transferred to LB supplemented with 50 μg/mL kanamycin agar plates to select for correctly integrated plasmids. Counterselection for recombination of the plasmid out of the genome was performed using YT media (10 g/L tryptone, 5 g/L yeast extract) containing 25% sucrose as previously described (Johnson and Beckham, 2015). MyTaqTM HS Red Mix (Bioline) was used for colony PCR reactions to confirm gene replacements. **Table S1** contains detailed strain construction information.

2.7. Shake flask cultivations

Shake flask experiments were conducted with modified M9 minimal media (pH 7.2, 6.78 g/L Na_2HPO_4, 3 g/L KH_2PO_4, 0.5 g/L NaCl, 1 g/L NH_4Cl, 2 mM $MgSO_4$, 100 μM $CaCl_2$, and 18 μM $FeSO_4$) supplemented with 20 mM (3.26 g/L) *p*CA and 10 mM glucose (1.80 g/L). Optical density (OD_{600}) of cultures was measured at 600 nm using Beckman DU640 spectrophotometer (Beckman Coulter). *P. putida* strains were inoculated from glycerol stocks and incubated overnight in 5 mL of LB medium. The overnight culture was washed in the M9 medium prior to inoculation into 25-30 mL media in 125-mL baffled flasks at OD_{600} = 0.10 and grown at 30°C, 225 rpm for 72 hours. An additional 10 mM glucose was added to each flask after 12, 24, and 48 hrs. Samples were taken for quantification of metabolites by removing 1 mL of culture, centrifuging >17,000 x *g* for 2 minutes, filtering the supernatant through 0.2 μM syringe filters, and stored in glass vials prior to analysis by HPLC as described in *section 2.11*.

2.8. Nicotinamide cofactor ratio determinations

CJ475, CJ680, and CJ781 were cultivated as described above in M9 minimal medium supplemented with 20 mM glucose and 20 mM *p*CA. At 12 hours of cultivation, $NADP^+$/NADPH was measured with a commercial colorimetric kit (Sigma Cat. #MAK038). $NADP^+$ and NADPH was extracted following manufacturer instructions. Briefly, 2 mL of culture was centrifuged at 2,000 x *g* for 5 minutes at 0°C, the pellet was resuspended in 800 μL of extraction buffer, incubated on ice for 10 minutes, centrifuged at 10,000 x *g* for 10 minutes, and filtered through a 3 kDa molecular weight cut-off filter (Amicon® Cat. UFC500324) by centrifuging at 14,000 x *g* for 30 minutes at 4°C. $NADP_{total}$ and NADPH were measured in the MWCO filtrate following manufacturer instructions. $NADP^+$/NADPH was calculated as ($NADP_{total}$-NADPH)/NADPH where $NADP^+$ (%) = $NADP_{total}$-NADPH x 100%.

2.9. Intracellular PobA and PraI quantification

CJ475, CJ680, and CJ781 were cultivated as described above in M9 minimal medium supplemented with 20 mM glucose and 20 mM *p*CA. At 12 hours of cultivation (from the same cultivations utilized in *Section 2.8.*), 10 mL of culture was centrifuged at 4,800 x *g* for 10 minutes at 4°C, the supernatant was decanted, and cell pellets were quenched in liquid nitrogen. Pellets were stored at -20°C prior to analysis. For absolute quantification by liquid chromatography and tandem mass spectrometry (LC-MS/MS), pellets were lysed via bead beating in 250 μL of lysis buffer (4% SDS, 100 mM Tris pH 8.0), precleared by centrifugation at 21,000 x *g* for 10 minutes, and proteins quantified with a Nanodrop OneC spectrophotometer (Thermo Scientific). Samples were denatured at 90°C for 10 minutes, disulfides reduced with tris(2-carboxyethyl)phosphine (TCEP) (adjusted to 10 mM) at 60°C for 10 minutes and blocked via alkylation with iodoacetamide (adjusted to 30 mM) in the dark for 15 minutes. Proteins were then cleaned up with protein aggregation capture and digested with proteomics-grade trypsin (Pierce) as previously described (Batth et al., 2019; Seo et al., 2021).

Eleven heavy isotope-labeled ($^{13}C/^{15}N$ on C-terminal lysine and arginine residues) peptide targets specific to PobA or PraI were synthesized (Thermo Scientific) following an initial global proteome screen (Table S11). Peptide selection with Skyline v. 21.1.0.146 (MacLean et al., 2010) was based on the following criteria: they must be unique to each protein, no methionine and cysteine residues, no mis-cleavage or ragged ends, 6-25 amino acids long, and ideally be among the most abundant peptides identified in the global analysis. A master mix containing all labeled peptides was qualified by LC-MS/MS before spiking into each sample.

Prior to targeted LC-MS/MS analysis by parallel reaction monitoring (PRM), the samples with heavy-labeled peptides were filtered (10 kDa MWCO Vivaspin 500; Sartorius), vacuum-dried, and re-suspended in solvent A (5% acetonitrile, 95% H_2O, 0.1% formic acid). Three microliters of each sample – equivalent to 3 μg tryptic peptides and 500 fmol of each heavy-labeled peptide standard – were injected onto a 5 cm C18 trap column (Kinetex 5 μm; Phenomenex) in-line with a 75 μm ID nanospray emitter packed with 15 cm C18 resin (Kinetex 1.7 μm; Phenomenex) and analyzed by 1D LC-PRM across a 90 minute gradient using a Vanquish ultra-HPLC (UHPLC) coupled directly to an Orbitrap Q Exactive Plus mass spectrometer (Thermo Scientific) as previously described (Walker et al., 2020; Walker, 2021).

The LC-PRM data were imported into Skyline to analyze, filter, and validate detection of both endogenous and heavy-labeled peptides (MacLean et al., 2010). Transitions not used for quantification were removed for each peptide and peak area boundaries were manually inspected and adjusted where necessary to ensure accurate peak assignment and peak areas. Library correlation for the precursors were

largely above 90% (Dot product). Proteotypic peptides met the following conditions: co-elution of the heavy and endogenous peptides; and similar transition ratios between the heavy and endogenous versions (Figure S4). One peptide for each PobA and PraI could not be quantified, but the nine remaining provided accurate quantitation of each protein target (Table S11). The peptide area ratio between the endogenous peptides to their corresponding heavy version was calculated by Skyline. Endogenous peptide concentration was calculated by multiplying the peptide area ratio by the amount of the heavy peptides injected (500 fmol) divided by the inject volume. PobA and PraI protein concentrations were calculated as the average of all their respective peptide concentrations.

2.10. Strain evaluation in bioreactors

Seed cultures for *P. putida* CJ475, CJ680, and CJ781 were prepared from glycerol stocks as follows. The surface of glycerol stocks was scraped and inoculated into 250 mL baffled flasks containing 50 mL of LB (Miller) media. These flasks were incubated for 16 hours at 30°C and 225 rpm. Then, the broths were centrifuged (8 minutes at 5,000 x *g*), the supernatant discarded, and the cells resuspended in modified M9 minimal medium for inoculation in the bioreactors (5 mL) at an initial OD_{600} of 0.2. The M9 bioreactor media consists of 13.55 g/L Na_2HPO_4, 6 g/L KH_2PO_4, 1 g/L NaCl, 2.25 g/L $(NH_4)_2SO_4$, 0.24 g/L $MgSO_4$, 11 mg/L $CaCl_2$, and 2.73 mg/L $FeSO_4$ (anhydrous). The higher concentration of media used in the bioreactor run was used to afford higher buffering capacity.

The bioreactors utilized in this study were 0.5 L BioStat-Q Plus bioreactors (Sartorius Stedim Biotech) and the cultivations involved a batch and a fed-batch phase. The media utilized in the batch phase was modified M9 as described above with the addition of glucose (2.7 g/L) as a carbon and energy source. The volume of the batch media was 250 mL. The bioreactors were controlled at 30°C and at pH 7 by the addition of 4 N NaOH, and air was sparged at 1 vvm. The initial agitation in the batch phase was 350 rpm and the dissolved oxygen (DO) was 100%. Subsequently, the DO was automatically controlled at 30% by agitation. At the 4 hour point in the batch phase, 2 mM *p*CA was added to induce the expression of aromatic catabolic enzymes in *P. putida* (Salvachua et al., 2020b). Once glucose was depleted in the batch phase, indicated as a rapid increase in DO levels, the fed-batch phase was initiated. The feeding media (250 mL) for the fed-batch phase contained 123 g/L (0.75 M) *p*CA AKSci (AK Scientific), 67.5 g/L glucose (0.37 M), 13.5 g/L $(NH_4)_2SO_4$ (0.1 M), and 4 mL/L antifoam 204. The feeding solution was adjusted to pH 9 with 10 N NaOH. Initial feeding rates were adjusted to feed 6, 9, 12, or 15 mmol *p*CA per hour and the fegieding rate was constant during the cultivations. Bioreactor experiments were performed in duplicate and samples (1.5 mL) were taken periodically to analyze bacterial growth (OD_{600}) and to measure the metabolites via HPLC as described in *section*

2.11. Quantification of metabolites

Cis,cis-muconic acid and aromatic acid quantitation was acheived by HPLC (Salvachúa et al., 2018). Subsequent to the work from (Bentley et al., 2020), *cis,cis*- and *cis,trans*-muconate isomers and aromatic acids were quantified utilizing the standard preparation outlined in (Black et al., 2019) and isocratic chromatography or the following equivalent adapted UHPLC chromatography. An Agilent 1290 UHPLC system (Agilent Technologies) equipped with a G7117A diode array detector was used for analysis. Separation was achieved using a Luna C18(2)-HST column 2.5 µm, 2 × 100 mm (Phenomenex) maintained at 45°C and mobile phase consisting of (A) 0.16% formic acid in water and (B) acetonitrile held at a constant flow rate of 0.5 mL/minute. Analytes were eluted using the following gradient program: starting conditions being (B) at 0% and held for 1 min, increased to 50% at 7.67 minutes, 70% at 9.33 minute and held at 70% until 10.67 minutes, returning to initial conditions at 10.68 minutes and held for column equilibration for a total run time of 13 minutes. Samples and standards were injected at volume of 1.0 µL and a calibration verification standard was run every 10-20 samples to monitor instrument drift.

Separation and quantitation of glucose was carried out by HPLC equipped with a refractive index detector (RID) previously detailed in (Bentley et al., 2020) utilizing a Shodex SP0810 sugar column or by an HPLC system coupled with a BioRad Aminex HPX-87H 9 µm, 7.8 × 300 mm column (BioRad). The Aminex column and RID were held at 55°C and chromatography was completed on samples and standards injected at a volume of 6 µL using 0.01 N sulfuric acid held at a constant flow rate of 0.6 mL/minute for a total run time of 27 minutes.

3. Results

3.1. PraI has a broader nicotinamide cofactor preference than PobA

We first characterized PobA and PraI *in vitro* to provide a baseline comparison of these two enzymes. Despite their use in metabolic engineering, a systematic *in vitro* kinetic comparison between the PobA and PraI has not been reported. To this end, PobA and PraI were heterologously produced in *E. coli* and purified to homogeneity. The purified enzymes appeared yellow, consistent with the presence of the FAD cofactor. The *in vitro* activity assays confirmed the nicotinamide cofactor preferences for PobA and PraI (Hosokawa and Stanier, 1966; Kasai et al., 2009). The addition of NADPH, but not NADH, elicited oxygen consumption in a mixture containing PobA and 4-HBA (**Figure 2A**). PobA, like the PHBH enzymes from *P. aeruginosa* and *P. fluorescens*, only accepts NADPH as the sole source of reducing equivalent and is unreactive toward NADH (Entsch and Ballou, 1989; Howell et al., 1972; Westphal et al., 2018). By contrast, addition of either NADPH or NADH to a mixture containing PraI and 4-HBA resulted in oxygen consumption, consistent with prior work (**Figure 2B**) (Kasai et al., 2009)

3.2. PobA and PraI hydroxylate 4-HBA at unity coupling

The reaction stoichiometry, defined here as the molar equivalencies between the consumptions of 4-HBA, O_2, and the production of PCA, were confirmed using a combination of oxygraph and HPLC assays. Both PobA and PraI have a near unity stoichiometry for all the associated reaction components (**Table S5**). In agreement with tight coupling, the turnover number (k_{cat}) for PobA and PraI are the same

when the three co-substrates were varied individually (*vide infra*).

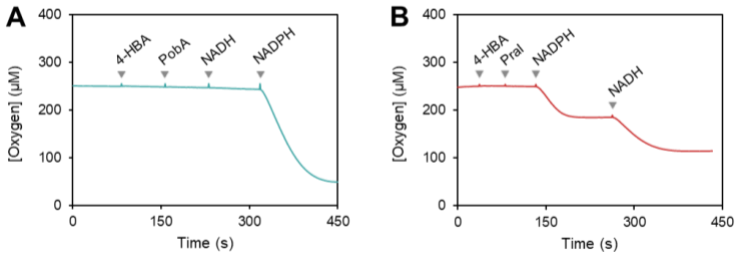

Figure 2. NAD(P)H specificities of PobA and PraI. Progress curves in a standard oxygraph assay describing the pyridine nicotinamide cofactor specificities of PobA (A, teal) and PraI (B, pink). PobA, PraI, 4-hydroxybenzoate, and NAD(P)H were added at the indicated points.

3.3. PobA and PraI transform 4-HBA with comparable specificities

Chloride ions have been previously shown to be inhibitory towards the enzymatic activity of PHBH and flavoprotein oxygenase in general (Meneely and Lamb, 2007; Steennis et al., 1973); thus, PHBH kinetic assays were performed in Tris/SO_4 pH 8 where PobA and PraI exhibit Michaelis-Menten kinetics, and no substrate inhibition was observed. Moreover, this buffer was used in prior studies and thus enables comparison to the kinetic parameters reported for other PHBHs (Entsch and Ballou, 1989; Eppink et al., 1998a). To account for a potentially lowered cofactor occupancy in the heterologously produced enzymes, the kinetic buffer was supplemented with FAD.

The steady-state kinetic analyses are summarized in **Table 1**. The comparison between the two assay methods showed systematically lower K_M values obtained using the spectroscopic methods. This slight bias may reflect the different sensitivity and response rate of the instruments. The overall steady-state kinetic parameters agree with the established observations in other PHBHs, where the K_M values are ordered incrementally in the following fashion: 4-HBA, NAD(P)H, and O_2 (Entsch and Ballou, 1989; Hesp et al., 1969; Hosokawa and Stanier, 1966; Howell et al., 1972). This ordering is consistent with the proposed catalytic mechanism where 4-HBA binds first and improves the rate of FAD reduction by NAD(P)H for the subsequent O_2 activation (Entsch and Ballou, 1989; Howell et al., 1972). Evaluation of the K_M of the O_2 implies that the kinetic parameters obtained with respect to 4-HBA, and NAD(P)H are apparent values as they were tested using air-saturated buffer (~3-4 × K_M); however, equivalent k_{cat} values obtained under various O_2, 4-HBA, and NAD(P)H concentrations suggest that the reported numbers are close to the true K_M values.

The steady-state kinetic parameters described in this study are comparable to reported values for other PHBHs. More specifically, the parameters for the heterologously-produced PobA are similar to the natively produced PHBHs from *P. aeruginosa* (k_{cat} = 63 s^{-1}; $K_M^{4\text{-HBA}}$ = 11 μM; K_M^{NADPH} = 23 μM; K_M^{oxygen} = 37 μM) and *P. fluorescens* (k_{cat} = 55 s^{-1}; $K_M^{4\text{-HBA}}$ = 25 μM; K_M^{NADPH} = 50 μM) (Entsch and Ballou, 1989; Eppink et al., 1998a; Husain and Massey, 1979). Overall, both PobA and PraI have similar catalytic efficiencies towards NADPH and the differences are on average less than a two-fold change under the different combination of the reactants. Comparing the catalytic efficiencies of PraI for the two forms of reducing equivalents indicated a slight preference towards NADPH, which is in contrast to a prior description of an apparent preference of PraI towards NADH (Kasai et al., 2009).

Table 1. Steady-state kinetic parameters of PobA and PraI. Experiments were performed using 50 mM Tris/SO_4, pH 8 supplemented with 60 μM FAD, at 25°C. Parameters were calculated using a minimum of 25 data points using Leonora. The experiments were performed using 200 μM 4-HBA, 300 μM NAD(P)H, and air-saturated buffer unless that the concentration of that substrate was varied. Two detection methods were used for the kinetic assays: spectrophotometrically by monitoring the loss of NAD(P)H signal at 340 nm and using an oxygraph following the depletion of O_2. Numerical data are provided in **Table S6A-E**.

reducing equivalent	enzyme	substrates: O_2 k_{cat} (s^{-1})	O_2 K_M (μM)	O_2 k_{cat}/K_M ($\times 10^5$ $s^{-1}.M^{-1}$)	4-hydroxybenzoate k_{cat} (s^{-1})	4-hydroxybenzoate K_M (μM)	4-hydroxybenzoate k_{cat}/K_M ($\times 10^5$ $s^{-1}.M^{-1}$)	NAD(P)H k_{cat} (s^{-1})	NAD(P)H K_M (μM)	NAD(P)H k_{cat}/K_M ($\times 10^5$ $s^{-1}.M^{-1}$)	detection method
NADPH	PobA	-	-	-	54 ± 5	18 ± 2	30 ± 4	50 ± 5	43 ± 3	12 ± 1	NADPH
		53 ± 5	70 ± 5	7.6 ± 0.7	40 ± 4	21 ± 1	19 ± 2	47 ± 4	66 ± 6	7.1 ± 0.7	O_2
	PraI	-	-	-	27 ± 3	16 ± 1	17 ± 2	27 ± 2	27 ± 1	10 ± 1	NADPH
		25 ± 2	68 ± 6	3.7 ± 0.3	23 ± 2	19 ± 2	19 ± 2	23 ± 2	33 ± 2	6.9 ± 0.7	O_2
NADH		-	-	-	26 ± 2	18 ± 1	14 ± 1	25 ± 2	49 ± 3	5.1 ± 0.5	NADH
		22 ± 2	54 ± 5	4.0 ± 0.4	21 ± 2	16 ± 1	13 ± 1	22 ± 2	46 ± 4	4.8 ± 0.6	O_2

3.4. PraI is structurally similar to other PHBHs

To gain a better insight into the differing cofactor specificities, a crystal structure of PraI was solved for comparison with PobA and other structurally characterized PHBHs (Gatti et al., 1996; Lazar et al., 2019; Ortiz-Maldonado et al., 1999; Schreuder et al., 1989; Schreuder et al., 1988). Notably, all PHBH structures described to date belong to the NADPH-specific group. PraI shares ~53% sequence identity with the PHBHs of *P. fluorescens*, *P. aeruginosa*, and *P. putida* for which several ligand-bound complex structures exist (**Figure S1B**). Consequently, PraI is structurally similar to the *Pseudomonas* PHBHs with root-mean-square deviation (RMSD)-values of ≤ 1.3 Å (Dali server (Holm, 2020)) (Gatti et al., 1996; Lazar et al., 2019; Ortiz-Maldonado et al., 1999; Schreuder et al., 1989) and exhibits a dimeric assembly with bound cofactor FAD and substrate 4-HBA (**Figure 3A**, **Table S7**) as well as retains the three domains architecture of PHBHs: domain I - FAD & NAD(P)H binding domain (residues 1-176), domain II - monooxygenase & 4-HBA binding domain (residues 177-294); and domain III - strictly α-helical oligomerization domain (residues 295-393) (**Figure S2**) (Entsch et al., 2005). Other than slight variations in the length of the secondary structure elements, the structural differences in PraI are primarily localized to its domain II. Nevertheless, comparison between the active sites revealed an absolute conservation for the residues that directly interact with 4-HBA (**Figure 3A**). Specifically, the carboxyl-group of 4-HBA forms a salt bridge with R216 and hydrogen bonding interactions with S214 and Y224, and the phenol group of 4-HBA is stabilized by interactions with the side chain of Y203 and the carbonyl backbone of P295 and T296. One of the hallmarks of the PHBH catalytic cycle is the mobility of the flavin cofactors that permits the use of a reactive flavin C4a-hydroxyperoxide species and its protection from solvent exposure thus preventing reaction uncoupling (Gatti et al., 1994; Schreuder et al., 1994). The isoalloxazine moiety of the FAD may adopt an IN or an OUT configurations as afforded by the flexible ribityl backbone and supported by the protein conformational changes (Brender et al., 2005). Like most PHBH structures, the FAD in our structure adopts an IN conformation where the isoalloxazine moiety is next the 4-HBA and is poised for the oxidative half-reaction (**Figure S3**) (Schreuder et al., 1988). This conformation is in contrast with the OUT conformation that is associated with the reductive half-reaction by allowing the flavin to access NAD(P)H for the hydride transfer reaction (Gatti et al., 1994; Lazar et al., 2019; Schreuder et al., 1994). Overall, the structure of PraI is remarkably similar to other PHBH structures described to date and the differing cofactor preferences do not stem from the conserved active site architecture.

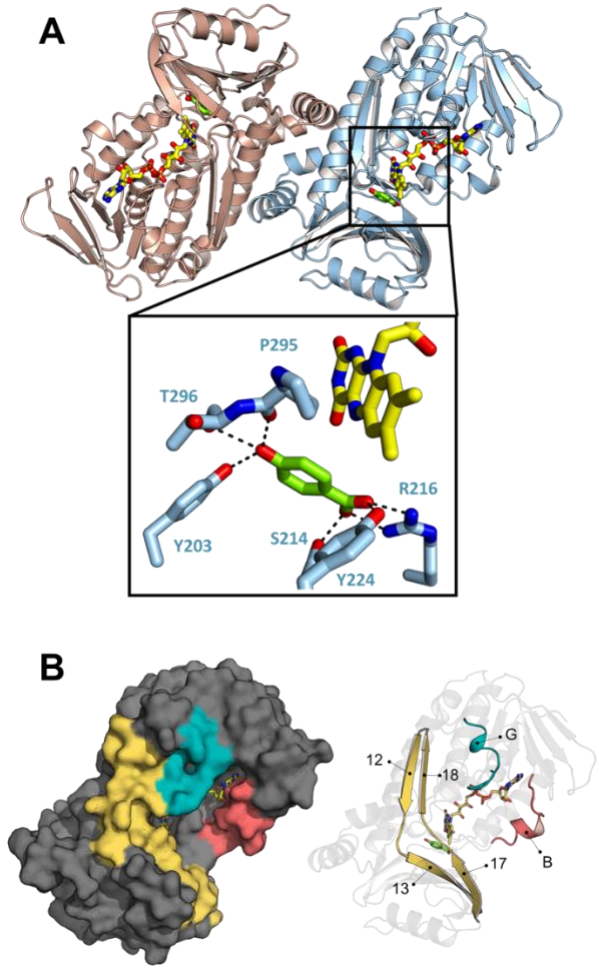

Figure 3. Crystal structure of PraI. (**A**) Dimeric assembly and active site of PraI. Protein interactions are shown with the bound 4-HBA (green) and FAD (yellow). Polar / hydrogen bond interactions are shown in black dashed lines. (**B**) Surface (left) and cartoon (right) representations of the inter-domain regions lining the entrance to the active site of PraI. The regions corresponding to helix-B (pink), helix-G (teal), and β-strands 12, 13, 17, and 18 (yellow) are highlighted.

3.4. Flexible interdomain regions of PraI may contribute towards a broader cofactor utilization

Despite the extensive kinetic and structural studies, the interaction between pyridine nicotinamide cofactor and PHBH remains an open question. This interaction is transient in nature and current understanding is limited due to the lack of a structural description of a NAD(P)H-bound PHBH complex (Entsch et al., 2005; Westphal et al., 2018). Indeed, there is a R220Q *Pa*PHBH structure with NADPH bound (Wang et al., 2002); however, this binding mode is likely to be non-productive as the pyridine group, the hydride donor, of NADPH points away from the isoalloxazine of the FAD. To that end, most of the models of NAD(P)H and PHBH complexes are generated through docking and computational studies as guided by various mutational analyses. Nonetheless, there is a growing line of evidence that the interdomain regions gating the cleft leading

to the active site, helix-B, helix-G, and β-strands 17 and 18 (**Figures 3B, S1A, S2B**), are responsible for the pyridine nicotinamide cofactor selectivity (Eppink et al., 1998b; Wang et al., 2002). Of these three sites, the helix-B region, also referred to as H2-helix in other studies, has been implicated with the cofactor preference the most (**Figure 3B, pink**) from extensive mutational and phylogenetic analyses (Eppink et al., 1998a; Eppink et al., 1999; van Berkel et al., 1988; Westphal et al., 2018). The helix-B region of PobA (ERQTAEYVLGR) matches the consensus sequence defined for the NADPH-specific PHBH; by contrast, the helix-B region of PraI (residue 32-42 in PraI, ENRTREEIEGT) matches that of the NADH-preferring PHBHs (**Figure S4**) (Westphal et al., 2018). The substitution of the last arginine of the helix-B for the NADPH-specific system (R42 in *Pf*PHBH) resulted in variants with lower affinities towards NADPH thereby highlighting its importance in cofactor binding (Eppink et al., 1998a). This position is substituted to a threonine (T42) in PraI. Nevertheless, a structural superposition of this region reveals that the conserved arginine side chain (R34) is oriented similarly and thus could substitute for the missing arginine at the end of helix-B (**Figure S4**). Furthermore, prior work swapping the helix-B from the NADPH-specific to NADH-utilizing sequences, was successful in flipping the pyridine nucleotide selectivity (Eppink et al., 1999); however, this change adversely affects the protein stability and lowered its activity significantly. Additionally, there exist other PHBHs with helix-B sequences that differ to the aforementioned motifs which suggests that while typical, they are not necessarily diagnostic for the cofactor preference (Westphal et al., 2018). Residue R164 in PraI is the most prominent residue within the helix-G region (residue 161-171 in PraI) (**Figure 3B, teal**). This position is substituted to a histidine in NADPH-specific PHBHs and was shown to be important for NADPH interaction by potentially binding to its pyrophosphate moiety (**Figure S5**) (Eppink et al., 1998b). Further, substitution of H162 to arginine in *Pf*PHBH resulted in a variant with similar activity to its wild-type counterpart, while a less conservative substitution led to a weaker affinity towards NADPH (Eppink et al., 1998b). Unfortunately, the H162R variant of *Pf*PHBH was not reported for its capacity to accept NADH as a cofactor. Considering the proximity and the orientation of the isoalloxazine moiety of the FAD to the β-strands 17 and 18 (residue 262 – 276 in PraI), the residue makeup of this region likely plays an important role for cofactor recognition and binding (**Figure 3B, yellow**). Adjacent to the β-strands 17 and 18 are the β-strands 12 and 13 (residue 177 – 293 in PraI) and together they mark the C and N termini of domain II in PHBHs, respectively. Both the β-strands 12 and 13 as well as β-strands 17 and 18 are two separate strands in PraI and connected with a flexible loop. By contrast, each β-strand pairs are contiguous in other PHBH structures (**Figure S6**) (Gatti et al., 1996; Lazar et al., 2019; Ortiz-Maldonado et al., 1999; Schreuder et al., 1989; Schreuder et al., 1988). Closer study of the residues between β-strands 17 and 18 in PraI reveals the presence of a conserved proline residue in non-PraI structures that introduce an added level of rigidity in this region. Conversely, the sequences for the β-strands 12 and 13 are conserved and the split might be a consequence of interactions with the β-strands 17 and 18. Notably, the arginine residue (R217 in PraI) adjacent to the β-strands 17 and 18 connecting loop is conserved in all known PHBH structures and has also been implicated in binding pyrophosphate of the pyridine nucleotide (Eppink et al., 1998b). Together, the higher flexibility afforded by the splitting of β-strands 12 and 13 and β-strands 17 and 18 in PraI may contribute towards its pyridine nicotinamide promiscuity. Overall, the PraI structure here is the first reported of an NADPH and NADH utilizing PHBH to our knowledge, and the differing cofactor specificity is attributable in part to the identity of the interdomain regions.

3.5. PraI substitution reduces 4-HBA accumulation during pCA conversion to MA

Previously, we engineered *P. putida* to convert *p*CA and FA to MA generating strain CJ475 (**Figure 1, Table S1**) (Salvachúa et al., 2018). However, CJ475 accumulated up to ~10 mM 4-HBA at 12 hours of cultivation in shake flask experiments fed with 20 mM *p*CA and 10 mM glucose, with an additional 10 mM glucose added after 12, 24, and 48 hours to support growth (**Figure 4A**). A previous attempt to address this bottleneck by integrating a second copy of *pobA*, driven by the strong, constitutive *tac* promoter (P_{tac}) (Bagdasarian et al., 1983), was not successful (Salvachúa et al., 2018), so we next explored whether expression of *praI* might improve 4-HBA conversion. To do this, *praI* was integrated into the genome in the same locus where the second copy of *pobA* had been in CJ475, namely downstream of the P_{tac} and upstream of a second copy of *vanAB*, which encodes the native vanillate *O*-demethylase that was overexpressed in CJ475 to overcome vanillate accumulation. The resulting strain (CJ680, **Table S1**) exhibited a 50% reduction in 4-HBA accumulation at 12 hours of cultivation in shake flasks (**Figure 4B**), indicating that the introduction of *praI* led to a faster conversion of 4-HBA and improved the rate of MA production. To ascertain the relative contributions of PobA and PraI, *pobA* was deleted from CJ680, generating strain CJ781. Fortunately, CJ781 showed a further reduction in 4-HBA accumulation (**Figure 4C**), indicating that expression of PraI alone enabled faster 4-HBA conversion to PCA.

3.6. PraI substitution improves NADPH bioavailability for other cellular processes.

We sought to further understand the underlying cause for 4-HBA accumulation differences observed in CJ475, CJ680, and CJ781 *in vivo*. Considering PobA and PraI have different cofactor specificity (**Table 1, Figure 2**) – notably, that PobA requires NADPH whereas PraI accepts NADH and NADPH – we hypothesized that 4-HBA turnover in PobA-expressing strains may be limited by NADPH availability. To test this, we measured intracellular $NADP^+$ to NADPH ratios ($NADP^+$/NADPH) in CJ475, CJ680, and CJ781. $NADP^+$/NADPH was measured at 12 hours of shake flask cultivation in M9 minimal medium supplemented with 10 mM glucose and 20 mM *p*CA (**Figure S7**, **Table S9-10**). This timepoint was chosen as the strain was in an exponential growth phase and 4-HBA accumulation is maximal of the sampled timepoints (**Figure S7, Table S9-10**).

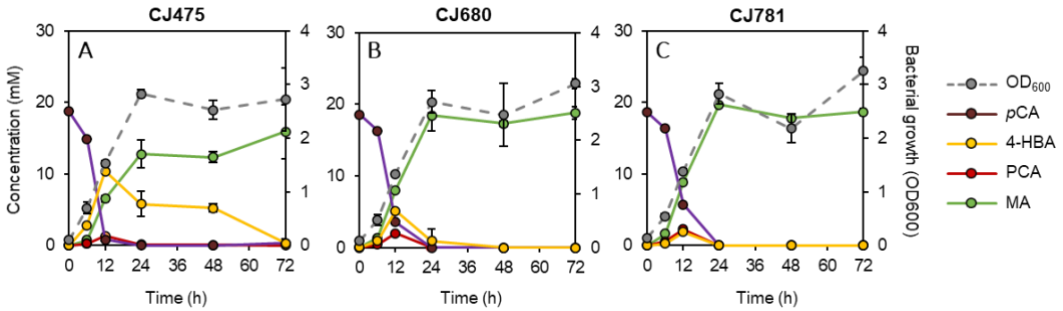

Figure 4. Shake flask cultivations of *P. putida* engineered for *p*CA conversion to MA via the intermediate 4-HBA. (**A**) CJ475 (expressing *pobA* only), (**B**) CJ680 (expressing *pobA* and *praI*), or (**C**) CJ781 (expressing *praI* only) cultivated in M9 minimal media containing 20 mM *p*CA and 10 mM glucose with an additional 10 mM glucose fed at 12, 24, and 48 h. Samples were taken periodically to measure growth and metabolite concentrations. The error bars represent standard deviation from three biological replicates. Full strain genotypes are provided in **Table S1**. Numerical data are provided in **Table S8**.

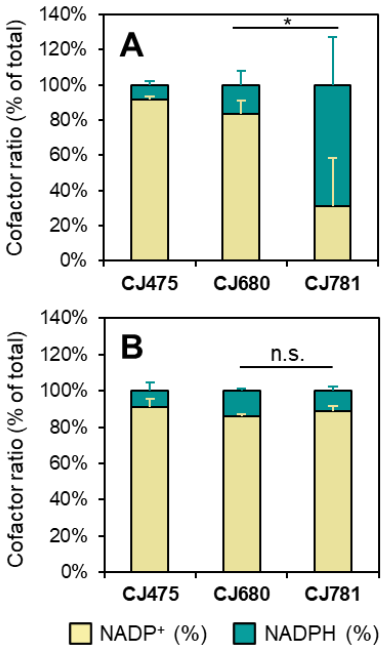

Figure 5. Percentage of the NADP(H) pool represented by NADP$^+$ and NADPH in *P. putida* strains CJ475, CJ680, and CJ781. Measurements were performed at 12 hours of cultivation in M9 minimal medium supplemented with (**A**) 20 mM *p*CA and 10 mM glucose or (**B**) 10 mM glucose. NADP$^+$ and NADPH are presented as a percentage of the total NADP(H) pool (see *Materials and Methods*). Error bars represent the standard deviation across biological triplicates each with technical duplicates. *p<0.05, paired one-tailed *t*-test. Full strain genotypes are provided in **Table S1**. Numerical data are provided in **Table S9**.

In CJ475 and CJ680 cultivations, NADPH represented 9 ± 2% and 17 ± 8% of the total NADP(H) pool (**Figure 5A**). Conversely, in CJ781 cultivations, NADPH represented 70 ± 30% of the total NAD(P)H pool, a significantly higher proportion relative to CJ680 (p < 0.05, paired one-tailed *t*-test, **Figure 5A**). NADP$^+$/NADPH ratios of 10 ± 3, 6 ± 5, and 0.5 ± 0.7 were observed for CJ475, CJ680, and CJ781, respectively. The elevation in NADPH observed in CJ781 is consistent with elevated NADPH production in *P. putida* strains grown in the presence of aromatic substrates (Nikel et al., 2015; Nikel et al., 2016b). A higher NADP$^+$/NADPH, indicative of lower NADPH availability, in CJ475 and CJ680 is consistent with the hypothesis that PobA-mediated 4-HBA hydroxylation was limited by NADPH. However, NADPH is required by many other cellular processes in addition to PHBH activity, so we considered whether the genetic background of a given strain, as opposed to PobA activity alone, could underpin these results. In cultivations with only glucose, NADP$^+$/NADPH was similar across all three strains (**Figure 5B**): NADPH (% of total) was 9 ± 4%, 14 ± 1%, and 11 ± 3% in CJ475, CJ680, and CJ781, respectively. Moreover, 4-HBA bottlenecks observed in CJ475 and CJ680 are attributable to NADP$^+$/NADPH imbalance, and thereby limited PHBH activity. Overall, the presence of PobA is detrimental as it competes for a futile 4-HBA transformation in CJ680 due to NADPH limitation.

3.7. PraI is highly overexpressed compared to PobA

We considered whether simply low PraI expression could be the reason for a lower NADP$^+$/NADPH ratio during *p*CA conversion to MA, as opposed to more balanced nicotinamide utilization during 4-HBA hydroxylation. *PobA* is expressed via native genetic elements in CJ475 and CJ680, whereas *praI* is expressed via the P_{tac} and a synthetic ribosome binding site (RBS) in CJ680 and CJ781. However, a prior study involving heterologous expression of *praI* in a non-native host observed poor translation rates stemming from the formation of hairpin loops near the RBS (Standaert et al., 2018). Thus, we sought to quantify intracellular PobA and PraI abundances in CJ475, CJ680, and CJ781. Each protein was quantified at 12 hours, the same time point that cofactor ratios were measured (**Figure 5**). Four and five unique labeled peptides were validated for quantitation of PobA and PraI, respectively (**Figures S8** and **S9**, **Table S11**) and added to extracted protein samples at a known abundance to enable absolute quantitation (see *Materials and Methods*).

As expected, PobA was expressed in CJ475 and CJ680 only when *p*CA was present (**Figure S10**). Interestingly, 6-fold more PraI than PobA was present in CJ680 cultivations in

*p*CA and glucose (0.6 ± 0.1 and 4 ± 0.7 μM PobA and PraI, respectively). A similar level of PraI was detected in *p*CA-containing cultivations of CJ781 (4.5 ± 0.5 μM) compared to CJ680 ($p = 0.28$). This result confirms that overexpression of PraI in *P. putida* was achieved, and further suggests that the increased relative NADPH availability in CJ781 is due to the absence of PobA rather than low expression of *praI*.

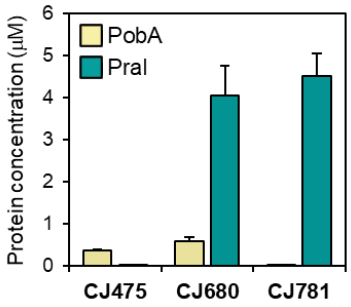

Figure 6. Intracellular PobA and PraI concentrations in *P. putida* strains CJ475, CJ680, and CJ781 after 12 hours of cultivation in M9 minimal medium supplemented with 20 mM glucose and 20 mM *p*CA. Four and five unique, validated labeled peptides were used for PobA and PraI measurements, respectively (**Figures S8** and **S9**). Error bars represent the standard deviation across biological triplicates. Full strain genotypes are provided in **Table S1**. Numerical data are provided in **Table S11.**

3.8. Substitution of PobA with PraI significantly improves MA productivity

Strain evaluation was next conducted in bioreactors to examine the effect of PraI expression on MA production in process relevant conditions, where differences in strain performance are often amplified. The bioreactor setup initially involves a batch phase in which the cells are grown on glucose and induced with *p*CA. The fed-batch phase initiation was coupled to the depletion of glucose at which point, this triggered the addition of a concentrated alkaline solution of *p*CA, glucose, and $(NH_4)_2SO_4$ (pH 9). To determine the appropriate feeding rate, we considered our shake flask experiment above and our previous work with *P. putida* CJ242 (which is equivalent to CJ475 without an additional copy of *vanAB*) where an increased *p*CA feed rates led to an accumulation of 4-HBA in CJ475, which indicates a metabolic bottleneck (Salvachúa et al., 2018). Based on these observations, we selected initial feeding rates of 6 and 9 mmol of *p*CA per hour to monitor the bottleneck in the 4-HBA conversion (Salvachúa et al., 2018).

With a feed of 6 mmol *p*CA per hour, CJ475 accumulated 4-HBA whereas CJ680 and CJ781 did not, which enabled an increased MA titer of 43 g/L while maintaining a 0.95 – 0.96 mol/mol yield for both strains (**Figure 7A-C**). To further enhance MA productivity, we increased feeding rates to 9 mmol of *p*CA per hour. 4-HBA accumulated in CJ475 when the feeding started (**Figure 7D**), similar to our previous results with CJ242 (Salvachúa et al., 2018). Conversely, 4-HBA did not accumulate in either CJ680 or CJ781 cultivations (**Figure 7E-F**). Despite overcoming the 4-HBA bottleneck, the strain performance of CJ680 and CJ781 exhibited notable differences. Specifically, while CJ680 accumulated *p*CA early in the cultivation (~24 h) (**Figure 7E**), CJ781 did not accumulate any *p*CA or any other catabolic intermediate, enabling a higher MA titer and productivity (**Figure 7F**) than both CJ680 at 9 mmol/h (**Figure 7E**) and CJ781 at 6 mmol/h (**Figure 7C**). Based on these results, we continued evaluating the effect of higher feeding rates (12 and 15 mmol *p*CA per hour) on MA production in CJ781 (**Figure S11**). *p*CA accumulated in the bioreactors as soon as the feeding initiated at both feeding rates which suggests the presence of an additional bottleneck likely related to *p*CA transport. Also, PCA – one of the most toxic aromatic catabolic intermediates in this pathway (Salvachúa et al., 2018) – accumulated up to 2.4 g/L which may represent an additional bottleneck upon the improvement of *p*CA transport.

4. Discussion and Conclusions

This study represents a continuation of previous metabolic engineering and bioprocess development studies focused on engineering *P. putida* toward industrially-relevant MA production from aromatic compounds (Johnson et al., 2016; Salvachúa et al., 2018; Sonoki et al., 2018; Vardon et al., 2015). In particular, we have focused on the hydroxycinnamic acids, *p*CA and FA, as substrates, which can be derived in yields up to ~25 wt% of the total lignin from corn stover and some grasses (Karlen et al., 2020; Karp et al., 2014; Karp et al., 2016; Karp et al., 2015; Ralph, 2010). The substrate of particular interest in this study, 4-HBA, is also found ester-linked to lignin and hemicellulose in some hardwoods in relatively high abundances (del Río et al., 2020), and the corresponding methoxylated substrate, vanillate, is a common product liberated from oxidative cleavage of ether linkages (Das et al., 2018; Rahimi et al., 2014; Schutyser et al., 2018). The work here overcomes a key bottleneck in the rate of 4-HBA conversion to the central intermediate, PCA, which can either be ring-opened directly (Fuchs et al., 2011), or as shown here, decarboxylated to catechol and ring-opened to MA. By addressing this bottleneck, we have improved the titer to 40 g/L MA at 100% molar yield using *p*CA as feed. We anticipate that the replacement of *pobA* with *praI* will also confer rate enhancements in strains that produce compounds via ring-opening with PCA or NADPH-intensive target products (Johnson et al., 2019; Notonier et al., 2021; Salvachua et al., 2020a), which will be studied in later work. In addition, we also endeavor to progressively increase the complexity the feedstock input starting from a defined aromatic mixture to a direct aromatic liquor as extracted from biomass while still maintaining high titer and yield to further improve the economic viability of the system.

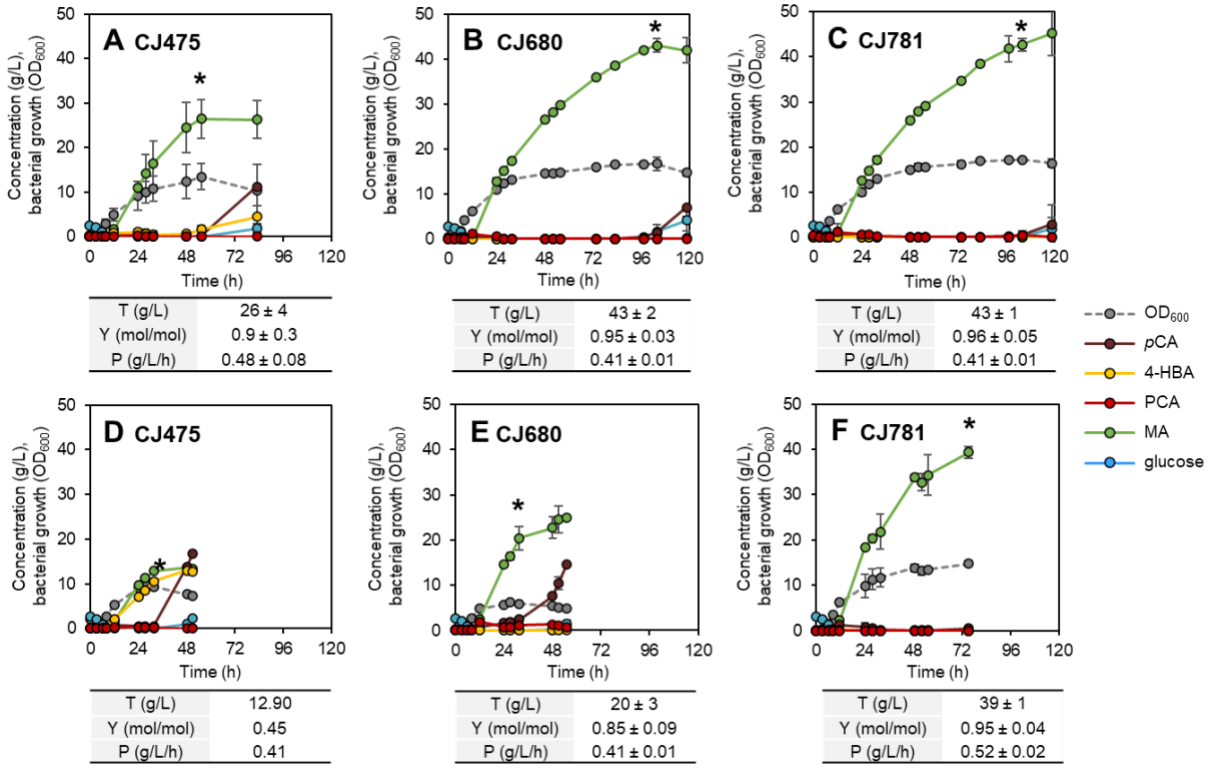

Figure 7. Bioreactor cultivations with CJ475, CJ680, and CJ781. *p*CA was fed at two different initial feeding rates in the fed-batch phase: (**A-C)** at 6 mmol/h and (**D-F**) at 9 mmol/h. Bacterial growth (OD_{600}), metabolite profiles, and MA titers (T), yields (Y), and productivities (P) are shown for each case. The asterisks indicate the time point at which T, Y, and P were calculated (either before *p*CA accumulated in the bioreactors or when the feeding was depleted). Profiles shown are the average of biological duplicates (excluding **D**, which is a single cultivation). Error bars show the absolute difference between the biological duplicates. Numerical data are provided in **Table S12**.

Additional metabolic engineering will be necessary to further improve MA productivity and titer. *p*CA accumulation in CJ781 bioreactors indicates a new bottleneck, potentially in *p*CA uptake. *p*CA and FA import is mediated in part by the aromatic acid/H^+ symporter HcnK (Wada et al., 2021). Furthermore, the hypothetical protein encoded by PP_3350 is implicated in *p*CA tolerance and resembles an outer membrane porin (Mohamed et al., 2020). Thus, modulation of *hcnK* and/or PP_3350 expression may serve as a viable strategy to increase *p*CA uptake. PCA accumulation, as observed in CJ781 bioreactor cultivations with ≥12 mmol *p*CA/h feeds, indicates another metabolic bottleneck. To overcome this, the heterologous PCA decarboxylation activity mediated by AroY, EcdD, and EcdB could be optimized by a variety of means. Notably, AroY requires a prFMN cofactor; engineering or laboratory evolution to optimize prFMN levels is a potentially promising strategy to improve heterologous AroY activity (Wang et al., 2018). Other strain optimization could also include means to improve the overall reduced cofactor pool, for example, by upregulating cytosolic or membrane-bound transhydrogenases that interconvert NADH and NADPH, which would be especially relevant for reactions with restrictive cofactor specificities (Spaans et al., 2015). Finally, MA titers may be limited by *P. putida* tolerance to MA. In this case, tolerance adaptive laboratory evolution (TALE) experiments, as done for *p*CA and FA tolerance (Mohamed et al., 2020), could reveal genetic engineering strategies to increase MA tolerance.

Aside from optimizing the cofactor levels for bioprocess optimization in this study, the cofactor preference in PHBH has garnered interest from the biochemical perspective as the enzyme lacks the canonical pyridine dinucleotide binding domain, unlike other NADPH-utilizing oxidoreductases (Mascotti et al., 2016; Sellés Vidal et al., 2018; van Berkel et al., 2006; Westphal et al., 2018). Interestingly, the primary sequence clustering of microbial PHBH has been shown to be largely driven by the cofactor preference rather than phylogeny and has been linked with the life cycle of the microbe with NADPH-specific PHBH associated more closely to the faster growing strains (Westphal et al., 2018). Furthermore, the NADPH-specific PHBH evolved later suggesting some form of specialization for the cofactor usage and that PHBH with a strict preference to NADH has not been reported to date to our knowledge (Westphal et al., 2018). Additional crystal structures of NADH-utilizing PHBH are necessary to ascertain the specifics in PraI structures. Specifically, whether the arginine in helix-G and the flexible β-strands 17 and 18 are sufficient in broadening the cofactor specificity. Nevertheless, the exact structural

description of a NAD(P)H-PHBH complex, perhaps through protein NMR, would be necessary to get a fuller picture of this interaction. Overall, the biochemical and structural characterization of PraI presented in this study provides an incremental step towards improving our collective understanding of how the pyridine nicotinamide specificity occurs in PHBH and the contribution of the interdomain regions remains to be explored.

Acknowledgements

This work was authored in part by the National Renewable Energy Laboratory, operated by Alliance for Sustainable Energy, LLC, for the U.S. Department of Energy (DOE) under Contract No. DE-AC36-08GO28308. EK, AZW, RJG, RLH, JEM, and GTB acknowledge funding from The Center for Bioenergy Innovation, a U.S. Department of Energy Research Center supported by the Office of Biological and Environmental Research in the DOE Office of Science. Funding was provided to CWJ, DS, CJS, CAS, SJH, SPW, KJR, and GTB by the U.S. Department of Energy Office of Energy Efficiency and Renewable Energy Bioenergy Technologies Office. MZ and JEM were supported by Research England through the Expanding Excellence in England (E3) scheme. The views expressed in the article do not necessarily represent the views of the DOE or the U.S. Government. The U.S. Government retains and the publisher, by accepting the article for publication, acknowledges that the U.S. Government retains a nonexclusive, paid-up, irrevocable, worldwide license to publish or reproduce the published form of this work, or allow others to do so, for U.S. Government purposes. We thank the Diamond Light Source for beamtime (proposal MX-23269) and the staff of beamline I03 for supporting automated data collection. Erika Erickson is thanked for the construction of pEE003. Veda S. Boorla and Costas D. Maranas are thanked for helpful discussions.

References

Abdelaziz, O. Y., Brink, D. P., Prothmann, J., Ravi, K., Sun, M., García-Hidalgo, J., Sandahl, M., Hulteberg, C. P., Turner, C., Lidén, G., Gorwa-Grauslund, M. F., 2016. Biological valorization of low molecular weight lignin. Biotechnology advances. 34**,** 1318-1346.

Almqvist, H., Veras, H., Li, K., Garcia Hidalgo, J., Hulteberg, C., Gorwa-Grauslund, M., Skorupa Parachin, N., Carlquist, M., 2021. Muconic acid production using engineered *Pseudomonas putida* KT2440 and a guaiacol-rich fraction derived from Kraft lignin. ACS Sustain. Chem. Eng. 9**,** 8097-8106.

Ankenbauer, A., Schäfer, R. A., Viegas, S. C., Pobre, V., Voß, B., Arraiano, C. M., Takors, R., 2020. *Pseudomonas putida* KT2440 is naturally endowed to withstand industrial-scale stress conditions. Microb. Biotechnol. 13**,** 1145-1161.

Bagdasarian, M. M., Amann, E., Lurz, R., Ruckert, B., Bagdasarian, M., 1983. Activity of the hybrid *trp-lac* (*tac*) promoter of *Escherichia coli* in *Pseudomonas putida*. Construction of broad-host-range, controlled-expression vectors. Gene. 26**,** 273-82.

Ballou, D. P., Entsch, B., Cole, L. J., 2005. Dynamics involved in catalysis by single-component and two-component flavin-dependent aromatic hydroxylases. Biochem. Biophys. Res. Commun. 338**,** 590-8.

Batth, T. S., Tollenaere, M. X., Rüther, P., Gonzalez-Franquesa, A., Prabhakar, B. S., Bekker-Jensen, S., Deshmukh, A. S., Olsen, J. V., 2019. Protein aggregation capture on microparticles enables multipurpose Proteomics Sample Preparation. Mol Cell Proteomics. 18**,** 1027-1035.

Becker, J., Wittmann, C., 2019. A field of dreams: Lignin valorization into chemicals, materials, fuels, and health-care products. Biotechnology advances. 37**,** 107360.

Beckham, G. T., Johnson, C. W., Karp, E. M., Salvachua, D., Vardon, D. R., 2016. Opportunities and challenges in biological lignin valorization. Curr. Opin. Biotechnol. 42**,** 40-53.

Belda, E., van Heck, R. G. A., José Lopez-Sanchez, M., Cruveiller, S., Barbe, V., Fraser, C., Klenk, H.-P., Petersen, J., Morgat, A., Nikel, P. I., Vallenet, D., Rouy, Z., Sekowska, A., Martins dos Santos, V. A. P., de Lorenzo, V., Danchin, A., Médigue, C., 2016. The revisited genome of *Pseudomonas putida* KT2440 enlightens its value as a robust metabolic chassis. Environ. Microbiol. 18**,** 3403-3424.

Bentley, G. J., Narayanan, N., Jha, R. K., Salvachúa, D., Elmore, J. R., Peabody, G. L., Black, B. A., Ramirez, K., De Capite, A., Michener, W. E., Werner, A. Z., Klingeman, D. M., Schindel, H. S., Nelson, R., Foust, L., Guss, A. M., Dale, T., Johnson, C. W., Beckham, G. T., 2020. Engineering glucose metabolism for enhanced muconic acid production in *Pseudomonas putida* KT2440. Metab. Eng. 59**,** 64-75.

Black, B. A., Michener, W. E., Payne, C. E., Beckham, G. T., Determination of *cis*,*cis*- and *cis*,*trans*-muconic acid from biological conversion. National Renewable Energy Laboratory, Golden, CO, 2019.

Boerjan, W., Ralph, J., Baucher, M., 2003. Lignin biosynthesis. Annu. Rev. Plant Biol. 54**,** 519-546.

Brender, J. R., Dertouzos, J., Ballou, D. P., Massey, V., Palfey, B. A., Entsch, B., Steel, D. G., Gafni, A., 2005. Conformational dynamics of the isoalloxazine in substrate-free *p*-hydroxybenzoate hydroxylase: single-molecule studies. J Am Chem Soc. 127**,** 18171-8.

Bricogne, G., Blanc, E., Brandl, M., Flensburg, C., Keller, P., Paciorek, W., Roversi, P., Sharff, A., Smart, O. S., Vonrhein, C., Womack, T. O., BUSTER Version 2.10.3. Global Phasing Ltd., Cambridge, United Kingdom, 2017.

Carraher, J. M., Pfennig, T., Rao, R. G., Shanks, B. H., Tessonnier, J.-P., 2017. *cis*,*cis*-Muconic acid isomerization and catalytic conversion to biobased cyclic-C6-1,4-diacid monomers. Green Chem. 19**,** 3042-3050.

Choi, K.-H., Kumar, A., Schweizer, H. P., 2006. A 10-min method for preparation of highly electrocompetent *Pseudomonas aeruginosa* cells: application for DNA

fragment transfer between chromosomes and plasmid transformation. J. Microbiol. Methods. 64**,** 391-397.

Clarkson, S. M., Giannone, R. J., Kridelbaugh, D. M., Elkins, J. G., Guss, A. M., Michener, J. K., 2017. Construction and optimization of a heterologous pathway for protocatechuate catabolism in *Escherichia coli* enables bioconversion of model aromatic compounds. Appl. Environ. Microbiol. 83.

Cornish-Bowden, A., 1995. Analysis of Enzyme Kinetic Data. Oxford University Press, Oxford, U. K.

Corona, A., Biddy, M. J., Vardon, D. R., Birkved, M., Hauschild, M. Z., Beckham, G. T., 2018. Life cycle assessment of adipic acid production from lignin. Green Chem. 20**,** 3857-3866.

Cywar, R. M., Rorrer, N. A., Hoyt, C. B., Beckham, G. T., Chen, E. Y. X., 2021. Bio-based polymers with performance-advantaged properties. Nat. Rev. Mater.

Das, A., Rahimi, A., Ulbrich, A., Alherech, M., Motagamwala, A. H., Bhalla, A., da Costa Sousa, L., Balan, V., Dumesic, J. A., Hegg, E. L., Dale, B. E., Ralph, J., Coon, J. J., Stahl, S. S., 2018. Lignin conversion to low-molecular-weight aromatics via an aerobic oxidation-hydrolysis sequence: comparison of different lignin sources. ACS Sustain. Chem. Eng. 6**,** 3367-3374.

Davis, R., Grundl, N., Tao, L., Biddy, M. J., Tan, E. C. D., Beckham, G. T., Humbird, D., Thompson, D. N., Roni, M. S., Process design and economics for the conversion of lignocellulosic biomass to hydrocarbon fuels and coproducts: 2018 biochemical design case update: biochemical deconstruction and conversion of biomass to fuels and products via integrated biorefinery pathways. National Renewable Energy Laboratory, Golden, CO, 2018.

Davis, R., Tao, L., Tan, E. C. D., Biddy, M. J., Beckham, G. T., Scarlata, C., Jacobson, J., Cafferty, K., Ross, J., Lukas, J., Knorr, D., Schoen, P., 2013. Process design and economics for the conversion of lignocellulosic biomass to hydrocarbons: dilute-acid and enzymatic deconstruction of biomass to sugars and biological conversion of sugars to hydrocarbons.

del Río, J. C., Rencoret, J., Gutiérrez, A., Elder, T., Kim, H., Ralph, J., 2020. Lignin monomers from beyond the canonical monolignol biosynthetic pathway: another brick in the wall. ACS Sustain. Chem. Eng. 8**,** 4997-5012.

Emsley, P., Lohkamp, B., Scott, W. G., Cowtan, K., 2010. Features and development of Coot. Acta Crystallogr. D Biol. Crystallogr. 66**,** 486-501.

Entsch, B., Ballou, D. P., 1989. Purification, properties, and oxygen reactivity of *p*-hydroxybenzoate hydroxylase from *Pseudomonas aeruginosa*. Biochim. Biophys. Acta. 999**,** 313-22.

Entsch, B., Cole, L. J., Ballou, D. P., 2005. Protein dynamics and electrostatics in the function of *p*-hydroxybenzoate hydroxylase. Arch. Biochem. Biophys. 433**,** 297-311.

Entsch, B., Van Berkel, W. J. H., 1995. Structure and mechanism of *para*-hydroxybenzoate hydroxylase. FASEB J. 9**,** 476-483.

Eppink, M. H., Schreuder, H. A., van Berkel, W. J., 1998a. Lys42 and Ser42 variants of *p*-hydroxybenzoate hydroxylase from *Pseudomonas fluorescens* reveal that Arg42 is essential for NADPH binding. Eur. J. Biochem. 253**,** 194-201.

Eppink, M. H. M., Overkamp, K. M., Schreuder, H. A., Van Berkel, W. J. H., 1999. Switch of coenzyme specificity of *p*-hydroxybenzoate hydroxylase. J. Mol. Biol. 292**,** 87-96.

Eppink, M. H. M., Schreuder, H. A., van Berkel, W. J. H., 1998b. Interdomain binding of NADPH in *p*-hydroxybenzoate hydroxylase as suggested by kinetic, crystallographic and modeling studies of histidine 162 and arginine 269 variants. J. Biol. Chem. 273**,** 21031-21039.

Frost, J. W., Draths, K. M., 1995. Biocatalytic syntheses of aromatics from D-glucose: renewable microbial sources of aromatic compounds. Annu. Rev. Microbiol. 49**,** 557-79.

Fuchs, G., Boll, M., Heider, J., 2011. Microbial degradation of aromatic compounds - from one strategy to four. Nat. Rev. Microbiol. 9**,** 803-16.

Gatti, D. L., Entsch, B., Ballou, D. P., Ludwig, M. L., 1996. pH-dependent structural changes in the active site of *p*-hydroxybenzoate hydroxylase point to the importance of proton and water movements during catalysis. Biochemistry. 35**,** 567-578.

Gatti, D. L., Palfey, B. A., Lah, M. S., Entsch, B., Massey, V., Ballou, D. P., Ludwig, M. L., 1994. The mobile flavin of 4-OH benzoate hydroxylase. Science. 266**,** 110-4.

Hesp, B., Calvin, M., Hosokawa, K., 1969. Studies on *p*-Hydroxybenzoate Hydroxylase from *Pseudomonas putida*. J. Biol. Chem. 244**,** 5644-5655.

Holm, L., 2020. DALI and the persistence of protein shape. Protein Sci. 29**,** 128-140.

Hosokawa, K., Stanier, R. Y., 1966. Crystallization and properties of *p*-hydroxybenzoate hydroxylase from *Pseudomonas putida*. J. Biol. Chem. 241**,** 2453-60.

Howell, L. G., Spector, T., Massey, V., 1972. Purification and properties of *p*-hydroxybenzoate hydroxylase from *Pseudomonas fluorescens*. J. Biol. Chem. 247**,** 4340-50.

Huang, K., Fasahati, P., Maravelias, C. T., 2020. System-level analysis of lignin valorization in lignocellulosic biorefineries. iScience. 23**,** 100751.

Huo, J., Shanks, B. H., 2020. Bioprivileged molecules: integrating biological and chemical catalysis for biomass conversion. Annu. Rev. Chem. Biomol. Eng. 11**,** 63-85.

Husain, M., Massey, V., 1979. Kinetic studies on the reaction of *p*-hydroxybenzoate hydroxylase. agreement of steady state and rapid reaction data. J. Biol. Chem. 254**,** 6657-66.

Jiménez, J. I., Miñambres, B., García, J. L., Díaz, E., 2002. Genomic analysis of the aromatic catabolic pathways from *Pseudomonas putida* KT2440. Environ. Microbiol. 4**,** 824-841.

Johnson, C. W., Abraham, P. E., Linger, J. G., Khanna, P., Hettich, R. L., Beckham, G. T., 2017. Eliminating a global regulator of carbon catabolite repression enhances the conversion of aromatic lignin monomers to muconate in *Pseudomonas putida* KT2440. Metab. Eng. Commun. 5**,** 19-25.

Johnson, C. W., Beckham, G. T., 2015. Aromatic catabolic pathway selection for optimal production of pyruvate and lactate from lignin. Metab. Eng. 28**,** 240-247.

Johnson, C. W., Salvachua, D., Khanna, P., Smith, H., Peterson, D. J., Beckham, G. T., 2016. Enhancing muconic acid production from glucose and lignin-derived aromatic compounds via increased protocatechuate decarboxylase activity. Metab. Eng. Commun. 3**,** 111-119.

Johnson, C. W., Salvachúa, D., Rorrer, N. A., Black, B. A., Vardon, D. R., St. John, P. C., Cleveland, N. S., Dominick, G., Elmore, J. R., Grundl, N., Khanna, P., Martinez, C. R., Michener, W. E., Peterson, D. J., Ramirez, K. J., Singh, P., VanderWall, T. A., Wilson, A. N., Yi, X., Biddy, M. J., Bomble, Y. J., Guss, A. M., Beckham, G. T., 2019. Innovative chemicals and materials from bacterial aromatic catabolic pathways. Joule. 3**,** 1523-1537.

Kabsch, W., Sander, C., 1983. Dictionary of protein secondary structure: pattern recognition of hydrogen-bonded and geometrical features. Biopolymers. 22**,** 2577-637.

Karlen, S. D., Fasahati, P., Mazaheri, M., Serate, J., Smith, R. A., Sirobhushanam, S., Chen, M., Tymokhin, V. I., Cass, C. L., Liu, S., Padmakshan, D., Xie, D., Zhang, Y., McGee, M. A., Russell, J. D., Coon, J. J., Kaeppler, H. F., de Leon, N., Maravelias, C. T., Runge, T. M., Kaeppler, S. M., Sedbrook, J. C., Ralph, J., 2020. Assessing the viability of recovery of hydroxycinnamic acids from lignocellulosic biorefinery alkaline pretreatment waste streams. ChemSusChem. 13**,** 2012-2024.

Karp, E. M., Donohoe, B. S., O'Brien, M. H., Ciesielski, P. N., Mittal, A., Biddy, M. J., Beckham, G. T., 2014. Alkaline pretreatment of corn stover: bench-scale fractionation and stream characterization. ACS Sustain. Chem. Eng. 2**,** 1481-1491.

Karp, E. M., Nimlos, C. T., Deutch, S., Salvachúa, D., Cywar, R. M., Beckham, G. T., 2016. Quantification of acidic compounds in complex biomass-derived streams. Green Chem. 18**,** 4750-4760.

Karp, E. M., Resch, M. G., Donohoe, B. S., Ciesielski, P. N., O'Brien, M. H., Nill, J. E., Mittal, A., Biddy, M. J., Beckham, G. T., 2015. Alkaline pretreatment of switchgrass. ACS Sustain. Chem. Eng. 3**,** 1479-1491.

Kasai, D., Fujinami, T., Abe, T., Mase, K., Katayama, Y., Fukuda, M., Masai, E., 2009. Uncovering the protocatechuate 2,3-cleavage pathway genes. J. Bacteriol. 191**,** 6758-68.

Kelley, L. A., Mezulis, S., Yates, C. M., Wass, M. N., Sternberg, M. J., 2015. The Phyre2 web portal for protein modeling, prediction and analysis. Nat. Protoc. 10**,** 845-58.

Kohlstedt, M., Starck, S., Barton, N., Stolzenberger, J., Selzer, M., Mehlmann, K., Schneider, R., Pleissner, D., Rinkel, J., Dickschat, J. S., Venus, J., B.J.H. van Duuren, J., Wittmann, C., 2018. From lignin to nylon: cascaded chemical and biochemical conversion using metabolically engineered *Pseudomonas putida*. Metab. Eng. 47**,** 279-293.

Lazar, J. T., Shuvalova, L., Rosas-Lemus, M., Kiryukhina, O., Satchell, K. J. F., Minasov, G., 2019. Structural comparison of *p*-hydroxybenzoate hydroxylase (PobA) from *Pseudomonas putida* with PobA from other *Pseudomonas* spp. and other monooxygenases. Acta Crystallogr. F Struct. Biol. Commun. 75**,** 507-514.

Linger, J. G., Vardon, D. R., Guarnieri, M. T., Karp, E. M., Hunsinger, G. B., Franden, M. A., Johnson, C. W., Chupka, G., Strathmann, T. J., Pienkos, P. T., Beckham, G. T., 2014. Lignin valorization through integrated biological funneling and chemical catalysis. Proc. Natl. Acad. Sci. U.S.A. 111**,** 12013-8.

Liu, Z.-H., Le, R. K., Kosa, M., Yang, B., Yuan, J., Ragauskas, A. J., 2019a. Identifying and creating pathways to improve biological lignin valorization. Renew. Sust. Energ. Rev. 105**,** 349-362.

Liu, Z.-H., Shinde, S., Xie, S., Hao, N., Lin, F., Li, M., Yoo, C. G., Ragauskas, A. J., Yuan, J. S., 2019b. Cooperative valorization of lignin and residual sugar to polyhydroxyalkanoate (PHA) for enhanced yield and carbon utilization in biorefineries. Sustain. Energy Fuels. 3**,** 2024-2037.

Lu, R., Lu, F., Chen, J., Yu, W., Huang, Q., Zhang, J., Xu, J., 2016. Production of diethyl terephthalate from biomass-derived muconic acid. Angew. Chem. Int. Ed. 55**,** 249-53.

MacLean, B., Tomazela, D. M., Shulman, N., Chambers, M., Finney, G. L., Frewen, B., Kern, R., Tabb, D. L., Liebler, D. C., MacCoss, M. J., 2010. Skyline: an open source document editor for creating and analyzing targeted proteomics experiments. Bioinformatics (Oxford, England). 26**,** 966-8.

Martin-Pascual, M., Batianis, C., Bruinsma, L., Asin-Garcia, E., Garcia-Morales, L., Weusthuis, R. A., van Kranenburg, R., Martins dos Santos, V. A. P., 2021. A navigation guide of synthetic biology tools for

Pseudomonas putida. Biotechnology advances. 49**,** 107732.

Mascotti, M. L., Juri Ayub, M., Furnham, N., Thornton, J. M., Laskowski, R. A., 2016. Chopping and changing: the evolution of the flavin-dependent monooxygenases. J. Mol. Biol. 428**,** 3131-3146.

McCoy, A. J., Grosse-Kunstleve, R. W., Adams, P. D., Winn, M. D., Storoni, L. C., Read, R. J., 2007. Phaser crystallographic software. J. Appl. Crystallogr. 40**,** 658-674.

Meneely, K. M., Lamb, A. L., 2007. Biochemical characterization of a flavin adenine dinucleotide-dependent monooxygenase, ornithine hydroxylase from *Pseudomonas aeruginosa*, suggests a novel reaction mechanism. Biochemistry. 46**,** 11930-7.

Mohamed, E. T., Werner, A. Z., Salvachua, D., Singer, C. A., Szostkiewicz, K., Rafael Jimenez-Diaz, M., Eng, T., Radi, M. S., Simmons, B. A., Mukhopadhyay, A., Herrgard, M. J., Singer, S. W., Beckham, G. T., Feist, A. M., 2020. Adaptive laboratory evolution of *Pseudomonas putida* KT2440 improves *p*-coumaric and ferulic acid catabolism and tolerance. Metab. Eng. Commun. 11**,** e00143.

Nikel, P. I., Chavarría, M., Danchin, A., de Lorenzo, V., 2016a. From dirt to industrial applications: *Pseudomonas putida* as a synthetic biology chassis for hosting harsh biochemical reactions. Curr. Opin. Chem. Biol. 34**,** 20-29.

Nikel, P. I., Chavarria, M., Fuhrer, T., Sauer, U., de Lorenzo, V., 2015. *Pseudomonas putida* KT2440 strain metabolizes glucose through a cycle formed by enzymes of the Entner-Doudoroff, Embden-Meyerhof-Parnas, and pentose phosphate pathways. J. Biol. Chem. 290**,** 25920-32.

Nikel, P. I., de Lorenzo, V., 2018. *Pseudomonas putida* as a functional chassis for industrial biocatalysis: From native biochemistry to trans-metabolism. Metab. Eng. 50**,** 142-155.

Nikel, P. I., Martínez-García, E., de Lorenzo, V., 2014. Biotechnological domestication of pseudomonads using synthetic biology. Nat. Rev. Microbiol. 12**,** 368-379.

Nikel, P. I., Perez-Pantoja, D., de Lorenzo, V., 2016b. Pyridine nucleotide transhydrogenases enable redox balance of *Pseudomonas putida* during biodegradation of aromatic compounds. Environ. Microbiol. 18**,** 3565-3582.

Notonier, S., Werner, A. Z., Kuatsjah, E., Dumalo, L., Abraham, P. E., Hatmaker, E. A., Hoyt, C. B., Amore, A., Ramirez, K. J., Woodworth, S. P., Klingeman, D. M., Giannone, R. J., Guss, A. M., Hettich, R. L., Eltis, L. D., Johnson, C. W., Beckham, G. T., 2021. Metabolism of syringyl lignin-derived compounds in *Pseudomonas putida* enables convergent production of 2-pyrone-4,6-dicarboxylic acid. Metab. Eng. 65**,** 111-122.

Okamura-Abe, Y., Abe, T., Nishimura, K., Kawata, Y., Sato-Izawa, K., Otsuka, Y., Nakamura, M., Kajita, S., Masai, E., Sonoki, T., Katayama, Y., 2016. Beta-ketoadipic acid and muconolactone production from a lignin-related aromatic compound through the protocatechuate 3,4-metabolic pathway. J. Biosci. Bioeng. 121**,** 652-658.

Ortiz-Maldonado, M., Gatti, D., Ballou, D. P., Massey, V., 1999. Structure−function correlations of the reaction of reduced nicotinamide analogues with *p*-hydroxybenzoate hydroxylase substituted with a series of 8-substituted flavins. Biochemistry. 38**,** 16636-16647.

Presley, G. N., Werner, A. Z., Katahira, R., Garcia, D. C., Haugen, S. J., Ramirez, K. J., Giannone, R. J., Beckham, G. T., Michener, J. K., 2021. Pathway discovery and engineering for cleavage of a beta-1 lignin-derived biaryl compound. Metab. Eng. 65**,** 1-10.

Ragauskas, A. J., Beckham, G. T., Biddy, M. J., Chandra, R., Chen, F., Davis, M. F., Davison, B. H., Dixon, R. A., Gilna, P., Keller, M., Langan, P., Naskar, A. K., Saddler, J. N., Tschaplinski, T. J., Tuskan, G. A., Wyman, C. E., 2014. Lignin valorization: improving lignin processing in the biorefinery. Science. 344**,** 1246843.

Rahimi, A., Ulbrich, A., Coon, J. J., Stahl, S. S., 2014. Formic-acid-induced depolymerization of oxidized lignin to aromatics. Nature. 515**,** 249-252.

Ralph, J., 2010. Hydroxycinnamates in lignification. Phytochem. Rev. 9**,** 65-83.

Ravi, K., Garcia-Hidalgo, J., Gorwa-Grauslund, M. F., Liden, G., 2017. Conversion of lignin model compounds by *Pseudomonas putida* KT2440 and isolates from compost. Appl. Microbiol. Biotechnol. 101**,** 5059-5070.

Salvachúa, D., Johnson, C. W., Singer, C. A., Rohrer, H., Peterson, D. J., Black, B. A., Knapp, A., Beckham, G. T., 2018. Bioprocess development for muconic acid production from aromatic compounds and lignin. Green Chem. 20**,** 5007-5019.

Salvachúa, D., Karp, E. M., Nimlos, C. T., Vardon, D. R., Beckham, G. T., 2015. Towards lignin consolidated bioprocessing: simultaneous lignin depolymerization and product generation by bacteria. Green Chem. 17**,** 4951-4967.

Salvachua, D., Rydzak, T., Auwae, R., De Capite, A., Black, B. A., Bouvier, J. T., Cleveland, N. S., Elmore, J. R., Furches, A., Huenemann, J. D., Katahira, R., Michener, W. E., Peterson, D. J., Rohrer, H., Vardon, D. R., Beckham, G. T., Guss, A. M., 2020a. Metabolic engineering of *Pseudomonas putida* for increased polyhydroxyalkanoate production from lignin. Microb. Biotechnol. 13**,** 813.

Salvachua, D., Werner, A. Z., Pardo, I., Michalska, M., Black, B. A., Donohoe, B. S., Haugen, S. J., Katahira, R., Notonier, S., Ramirez, K. J., Amore, A., Purvine, S.

O., Zink, E. M., Abraham, P. E., Giannone, R. J., Poudel, S., Laible, P. D., Hettich, R. L., Beckham, G. T., 2020b. Outer membrane vesicles catabolize lignin-derived aromatic compounds in *Pseudomonas putida* KT2440. Proc. Natl. Acad. Sci. U.S.A. 117**,** 9302-9310.

Schreuder, H. A., Mattevi, A., Obmolova, G., Kalk, K. H., Hol, W. G., van der Bolt, F. J., van Berkel, W. J., 1994. Crystal structures of wild-type p-hydroxybenzoate hydroxylase complexed with 4-aminobenzoate,2,4-dihydroxybenzoate, and 2-hydroxy-4-aminobenzoate and of the Tyr222Ala mutant complexed with 2-hydroxy-4-aminobenzoate. Evidence for a proton channel and a new binding mode of the flavin ring. Biochemistry. 33**,** 10161-70.

Schreuder, H. A., Prick, P. A. J., Wierenga, R. K., Vriend, G., Wilson, K. S., Hol, W. G. J., Drenth, J., 1989. Crystal structure of the *p*-hydroxybenzoate hydroxylase-substrate complex refined at 1.9 Å resolution: analysis of the enzyme-substrate and enzyme-product complexes. J. Mol. Biol. 208**,** 679-696.

Schreuder, H. A., van der Laan, J. M., Hol, W. G. J., Drenth, J., 1988. Crystal structure of *p*-hydroxybenzoate hydroxylase complexed with its reaction product 3,4-dihydroxybenzoate. J. Mol. Biol. 199**,** 637-648.

Schutyser, W., Kruger, J. S., Robinson, A. M., Katahira, R., Brandner, D. G., Cleveland, N. S., Mittal, A., Peterson, D. J., Meilan, R., Román-Leshkov, Y., Beckham, G. T., 2018. Revisiting alkaline aerobic lignin oxidation. Green Chem. 20**,** 3828-3844.

Sellés Vidal, L., Kelly, C. L., Mordaka, P. M., Heap, J. T., 2018. Review of NAD(P)H-dependent oxidoreductases: properties, engineering and application. Biochim. Biophys. Acta - Proteins Proteom. 1866**,** 327-347.

Seo, H., Lee, J.-W., Giannone, R. J., Dunlap, N. J., Trinh, C. T., 2021. Engineering promiscuity of chloramphenicol acetyltransferase for microbial designer ester biosynthesis. Metab. Eng. 66**,** 179-190.

Shanks, B. H., Keeling, P. L., 2017. Bioprivileged molecules: creating value from biomass. Green Chem. 19**,** 3177-3185.

Sonoki, T., Morooka, M., Sakamoto, K., Otsuka, Y., Nakamura, M., Jellison, J., Goodell, B., 2014. Enhancement of protocatechuate decarboxylase activity for the effective production of muconate from lignin-related aromatic compounds. J Biotechnol. 192 Pt A**,** 71-7.

Sonoki, T., Takahashi, K., Sugita, H., Hatamura, M., Azuma, Y., Sato, T., Suzuki, S., Kamimura, N., Masai, E., 2018. Glucose-free *cis,cis*-muconic acid production via new metabolic designs corresponding to the heterogeneity of lignin. ACS Sustain. Chem. Eng. 6**,** 1256-1264.

Spaans, S. K., Weusthuis, R. A., van der Oost, J., Kengen, S. W., 2015. NADPH-generating systems in bacteria and archaea. Front. Microbiol. 6**,** 742.

Standaert, R. F., Giannone, R. J., Michener, J. K., 2018. Identification of parallel and divergent optimization solutions for homologous metabolic enzymes. Metab. Eng. Commun. 6**,** 56-62.

Steennis, P. J., Cordes, M. M., Hilkens, J. G. H., Müller, F., 1973. On the interaction of *para*-hydroxybenzoate hydroxylase from *Pseudomonas fluorescens* with halogen ions. FEBS Lett. 36**,** 177-180.

Tickle, I. J., Flensburg, C., Keller, P., Paciorek, W., Sharff, A., Vorhein, C., Bricogne, G., STARANISO. Global Phasing Ltd., Cambridge, United Kingdom, 2018.

Touw, W. G., Baakman, C., Black, J., te Beek, T. A., Krieger, E., Joosten, R. P., Vriend, G., 2015. A series of PDB-related databanks for everyday needs. Nucleic Acids Res. 43**,** D364-8.

Tumen-Velasquez, M., Johnson, C. W., Ahmed, A., Dominick, G., Fulk, E. M., Khanna, P., Lee, S. A., Schmidt, A. L., Linger, J. G., Eiteman, M. A., Beckham, G. T., Neidle, E. L., 2018. Accelerating pathway evolution by increasing the gene dosage of chromosomal segments. Proc. Natl. Acad. Sci. U.S.A. 115**,** 7105-7110.

van Berkel, W. J., Kamerbeek, N. M., Fraaije, M. W., 2006. Flavoprotein monooxygenases, a diverse class of oxidative biocatalysts. J. Biotechnol. 124**,** 670-89.

van Berkel, W. J., Müller, F., Jekel, P. A., Weijer, W. J., Schreuder, H. A., Wierenga, R. K., 1988. Chemical modification of tyrosine-38 in *p*-hydroxybenzoate hydroxylase from *Pseudomonas fluorescens* by 5'-p-fluorosulfonylbenzoyladenosine: a probe for the elucidation of the NADPH binding site. Involvement in catalysis, assignment in sequence and fitting to the tertiary structure. Eur. J. Biochem. 176**,** 449-59.

van Duuren, J. B. J. H., de Wild, P. J., Starck, S., Bradtmöller, C., Selzer, M., Mehlmann, K., Schneider, R., Kohlstedt, M., Poblete-Castro, I., Stolzenberger, J., Barton, N., Fritz, M., Scholl, S., Venus, J., Wittmann, C., 2020. Limited life cycle and cost assessment for the bioconversion of lignin-derived aromatics into adipic acid. Biotechnol. Bioeng. 117**,** 1381-1393.

Vardon, D. R., Franden, M. A., Johnson, C. W., Karp, E. M., Guarnieri, M. T., Linger, J. G., Salm, M. J., Strathmann, T. J., Beckham, G. T., 2015. Adipic acid production from lignin. Energy Environ. Sci. 8**,** 617-628.

Vardon, D. R., Rorrer, N. A., Salvachúa, D., Settle, A. E., Johnson, C. W., Menart, M. J., Cleveland, N. S., Ciesielski, P. N., Steirer, K. X., Dorgan, J. R., Beckham, G. T., 2016. *cis,cis*-Muconic acid: separation and catalysis to bio-adipic acid for nylon-6,6 polymerization. Green Chem. 18**,** 3397-3413.

Wada, A., Prates, É. T., Hirano, R., Werner, A. Z., Kamimura, N., Jacobson, D. A., Beckham, G. T., Masai, E., 2021. Characterization of aromatic

acid/proton symporters in *Pseudomonas putida* KT2440 toward efficient microbial conversion of lignin-related aromatics. Metab. Eng. 64**,** 167-179.

Walker, C., Ryu, S., Giannone, R. J., Garcia, S., Trinh, C. T., 2020. Understanding and eliminating the detrimental effect of thiamine deficiency on the oleaginous yeast *Yarrowia lipolytica*. Appl. Environ. Microbiol. 86**,** e02299-19.

Walker, H. J., 2021. Chapter Nine - Metabolite imaging by mass spectrometry: A new discovery tool. In: Pétriacq, P., Bouchereau, A., Eds.), Advances in Botanical Research. vol. 98. Academic Press, pp. 271-296.

Wang, J., Ortiz-Maldonado, M., Entsch, B., Massey, V., Ballou, D., Gatti, D. L., 2002. Protein and ligand dynamics in 4-hydroxybenzoate hydroxylase. Proc. Natl. Acad. Sci. U.S.A. 99**,** 608.

Wang, P. H., Khusnutdinova, A. N., Luo, F., Xiao, J., Nemr, K., Flick, R., Brown, G., Mahadevan, R., Edwards, E. A., Yakunin, A. F., 2018. Biosynthesis and activity of prenylated FMN cofactors. Cell Chem. Biol. 25**,** 560-570 e6.

Weimer, A., Kohlstedt, M., Volke, D. C., Nikel, P. I., Wittmann, C., 2020. Industrial biotechnology of *Pseudomonas putida*: advances and prospects. Appl. Microbiol. Biotechnol. 104**,** 7745-7766.

Westphal, A. H., Tischler, D., Heinke, F., Hofmann, S., Groning, J. A. D., Labudde, D., van Berkel, W. J. H., 2018. Pyridine nucleotide coenzyme specificity of *p*-hydroxybenzoate hydroxylase and related flavoprotein monooxygenases. Front. Microbiol. 9**,** 3050.

Williams, C. J., Headd, J. J., Moriarty, N. W., Prisant, M. G., Videau, L. L., Deis, L. N., Verma, V., Keedy, D. A., Hintze, B. J., Chen, V. B., Jain, S., Lewis, S. M., Arendall, W. B., 3rd, Snoeyink, J., Adams, P. D., Lovell, S. C., Richardson, J. S., Richardson, D. C., 2018. MolProbity: More and better reference data for improved all-atom structure validation. Protein Sci. 27**,** 293-315.